Planetary and Space Science 59 (2011) 639–660

Contents lists available at ScienceDirect

Planetary and Space Science

journal homepage: www.elsevier.com/locate/pss

Review Article

In situ methods for measuring thermal properties and heat flux on planetary bodies

Norbert I. Kömle [a,*], Erika S. Hütter [a], Wolfgang Macher [a], Erika Kaufmann [a], Günter Kargl [a], Jörg Knollenberg [b], Matthias Grott [b], Tilman Spohn [b], Roman Wawrzaszek [c], Marek Banaszkiewicz [c], Karoly Seweryn [c], Axel Hagermann [d]

[a] *Space Research Institute, Austrian Academy of Sciences, Graz, Austria*
[b] *DLR Insitut für Planetenforschung, Berlin, Germany*
[c] *Space Research Centre, Polish Academy of Sciences, Warsaw, Poland*
[d] *Centre for Earth, Planetary, Space and Astronomical Research (CEPSAR), Open University, Milton Keynes, UK*

ARTICLE INFO

Article history:
Received 21 October 2010
Received in revised form
10 March 2011
Accepted 11 March 2011
Available online 21 March 2011

Keywords:
Thermal conductivity
Planetary surfaces
Lander missions

ABSTRACT

The thermo-mechanical properties of planetary surface and subsurface layers control to a high extent in which way a body interacts with its environment, in particular how it responds to solar irradiation and how it interacts with a potentially existing atmosphere. Furthermore, if the natural temperature profile over a certain depth can be measured *in situ*, this gives important information about the heat flux from the interior and thus about the thermal evolution of the body. Therefore, in most of the recent and planned planetary lander missions experiment packages for determining thermo-mechanical properties are part of the payload. Examples are the experiment MUPUS on Rosetta's comet lander *Philae*, the TECP instrument aboard NASA's Mars polar lander *Phoenix*, and the mole-type instrument HP^3 currently developed for use on upcoming lunar and Mars missions. In this review we describe several methods applied for measuring thermal conductivity and heat flux and discuss the particular difficulties faced when these properties have to be measured in a low pressure and low temperature environment. We point out the abilities and disadvantages of the different instruments and outline the evaluation procedures necessary to extract reliable thermal conductivity and heat flux data from *in situ* measurements.

Contents

* Corresponding author. Tel.: +43 316 4120651; fax: +43 316 4120690.
E-mail address: norbert.koemle@oeaw.ac.at (N.I. Kömle).

0032-0633 © 2011 Elsevier Ltd. Open access under CC BY-NC-ND license.
doi:10.1016/j.pss.2011.03.004

1. Introduction

The temperature distribution inside and near the surface of planetary bodies is determined by various factors (see e.g. Teisseyre and Leliwa-Kopystynski, 1992). First, it depends on the thermal energy produced inside the body as well as the energy received and absorbed from external radiation sources. The former consists of the heat dissipated during the formation phase of the planet and stored since then in the interior as well as on the heat produced by ongoing radioactive decay of unstable isotopes. These processes warm up a planetary body from the interior. The second contribution is the electromagnetic radiation emitted by the Sun and absorbed by the planetary surface or a planetary atmosphere, where it is finally dissipated into heat.

In order to find the temperature distribution and its evolution with time in the interior and near the surface of a planetary body one has to apply the physical laws by which the heat is distributed. There are three possible pathways how this can happen:

- *Thermal conduction*—taking place in solid, liquid, and gaseous materials. Here the energy is propagated by vibrations and chaotic motions of the molecules. Macroscopic material motions are absent in this mode.
- *Convection*—taking place only in liquid and gaseous materials. Here the energy is transported by macroscopic motions of liquids or gases, which can occur either in a smooth way (laminar flow) or in a quasi-chaotic way (turbulent flow). It can be considered as the most effective way of heat transport.
- *Radiation*—taking place in any body exhibiting internal or external surfaces. It is the only process that does not demand direct material contact between heat exchanging elements and therefore also the only way how different celestial bodies can exchange energy among each other (aside of solar wind and plasma interactions). But it is also the most ineffective process for exchanging heat, and therefore it is only important in the absence of the other possibilities.

From the above it follows that the way in which the energy generated in or absorbed by a planetary body is distributed as a function of space and time is highly dependent on the nature and structure of the body. Since we know that planets, comets, and asteroids have formed some 4.5 billion years ago by the accretion of a gas/dust cloud to planetesimals and finally to planets, it is clear that they have also a very complex thermal history, which has nowadays not yet come to an end. While the general trend is a gradual cooling of the planetary interiors in the course of time, this evolution also includes phases of partial or complete melting of large parts of planetary interiors, which allows all heat transfer mechanisms to be active.

To get a better understanding of the thermal structure and history of the planetary bodies in our Solar System (including Earth), extensive numerical modeling work is inevitable. However, in order to produce realistic results, any numerical model needs appropriate boundary and initial conditions as well as trustworthy material parameters. While—at least for Earth—seismological methods can be used to retrieve information on the present day interior structure, there are two other key parameters that cannot be derived from seismological observations: (i) The heat flux from the interior and (ii) the thermal properties of the near surface layers, in particular the thermal conductivity of these layers. The latter are especially important for bodies lacking an atmosphere, like the Moon, asteroids and Mercury (Hagermann, 2005).

This review will concentrate on the methods and instruments used in the past and developed for future missions to determine these two key parameters. Section 2 introduces the basic physical laws of heat transfer and the relevant material parameters controlling heat flow both in the interior and across boundaries. In Section 3 the theory needed for the evaluation of thermal conductivity measurements is reviewed and explicit formulae for various sensor configurations are given. Subsequently in Section 4 we describe laboratory prototypes of thermal conductivity sensors as well as instruments that have been developed and used for geophysical and planetary applications. Hereby some emphasis is given to recent and upcoming space missions e.g. the TECP instrument on NASA's *Phoenix* Mars lander, the MUPUS instrument on the Rosetta lander *Philae*, and the HP^3 instrument currently developed for applications on Moon and Mars. Finally, Section 5 presents a comparison of different designs and evaluation methods and gives some conclusions relevant for future developments.

2. Basics

The flow of heat from one point of a solid body to another is basically driven by the temperature differences existing inside and at the boundaries of the body. This property is expressed mathematically by Fourier's law of heat transfer:

$$\vec{F} = -\lambda \nabla T \tag{1}$$

The parameter λ (unit: W m^{-1} K^{-1}) determining heat flow along the direction of the temperature gradient is called *thermal conductivity*. In the simplest case, i.e. for a solid body with homogeneous structure, the variation of temperature T in space and time is described by the so-called *heat conduction* equation:

$$\varrho C_M \frac{\partial T}{\partial t} = \lambda \Delta T + g(\vec{r},t) \tag{2}$$

where the term $g(\vec{r})$ (unit: W m^{-3}) denotes the heat gain or loss term describing the thermal power generated or consumed in a unit volume by processes other than thermal conduction (for example heating by an electrical current flowing in the material or exothermal chemical reactions or phase changes). In contrast to the equation for the heat flow, this second order partial differential equation involves not only λ, but also two additional material parameters—density ϱ (unit: kg m^{-3}) and heat capacity per unit mass C_M (unit: J kg^{-1} K^{-1}). Multiplication of these two properties yields the volumetric heat capacity

$$C_V = \varrho\, C_M \tag{3}$$

(unit: J m^{-3} K^{-1}). In the formulae compiled below density and heat capacity always appear in the form (3), therefore we will usually write C_V instead of using ϱ and C_M as separate parameters.

Another combination of these three parameters which occurs frequently in the formulae is the so-called *thermal diffusivity* (unit: m^2 s^{-1}), which is analogous to a diffusion coefficient in

material flow:

$$\kappa = \frac{\lambda}{\varrho C_M} = \frac{\lambda}{C_V} \tag{4}$$

3. Theory of thermal sensors

In the following subsections we summarize known solutions of the heat conduction equation for axisymmetric configurations, which are commonly used to evaluate transient thermal conductivity measurements. It should be noted that the thermal conductivity sensors reviewed here are basically constructed to investigate *solid* materials. These include materials with a porous or grainy structure, containing voids filled by gases, as investigated e.g. by Hütter et al. (2008). They have also been used sometimes for pure gases or liquids, but in this case the possible influence of convective energy transport must be carefully considered (see e.g. Phylippov et al., 1992; Hathi et al., 2007, 2008). Most of the known solutions for the temperature field in axisymmetric configurations can be found in the classical book on heat conduction by Carslaw and Jaeger (1959) and in several other reference papers (Jaeger, 1941, 1956). Another important reference book giving the axisymmetric solutions of the heat conduction equation from a more generalized point of view is Özisik (1989). The fundamental methods to obtain these solutions involve the application of *Green functions* and the *Laplace transformation* in a cylindrical coordinate system (r,z,φ). Solutions can be typically expressed in terms of Bessel functions, as we will see below. In principle, by using the Green functions method, semi-analytical solutions are obtainable not only for the one-dimensional case (temperature T dependent only on the radial coordinate r and time t), but also for the general axisymmetric case ($T(r,z,t)$) and even for the fully three-dimensional case ($T(r,z,\varphi,t)$). Some years ago Banaszkiewicz (2002a–e) has compiled the solutions for all cases. However, the analytic formulae for the two- and three-dimensional cases become extremely lengthy and cumbersome to use. To our knowledge, they have hardly been used in practical work until now. Rather, solutions for long and thin cylinders are used extensively, even in cases where their uncritical application may be doubtful. In this review we will first compile the formulae for long and slender probes, where the temperature field depends only on r and t, and subsequently analyze the case of a sensor with arbitrary z-extension. While the Carslaw and Jaeger book contains most of the materials needed, we will follow here a more didactic presentation style, developing the relevant formulae step by step, from the simple to the more complex cases.

For the one-dimensional case the time-dependent heat conduction equation (2) takes the form

$$C_V \frac{\partial T}{\partial t} = \frac{1}{r}\frac{\partial}{\partial r}\left(\lambda r \frac{\partial T}{\partial r}\right) + g(r,t) \tag{5}$$

in the range $0 \le r < \infty$ and $t > 0$. In order to solve this equation for the temperature field $T(r,t)$, one has to define in addition initial and boundary conditions.

3.1. Formulae where sensor thermal properties are negligible

To start with, consider a point-like heat source embedded in an infinite solid medium with defined thermal properties. Hereby it is assumed that a finite amount of heat energy is released inside an infinitesimal volume within an infinitesimally short time. This situation is illustrated in the left side of Fig. 1.

According to Carslaw and Jaeger (1959), the temperature field in the three-dimensional space which develops as a function of time t in response to such a heat pulse is given as a solution of the heat conduction equation (2) by

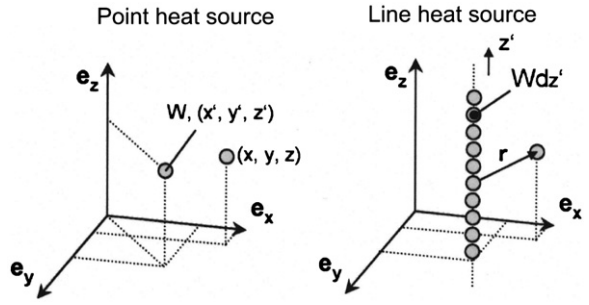

Fig. 1. Sketches of a point-like and a line-like heat source embedded in an infinite medium with defined thermal properties (after Hütter, 2007).

$$T(x,y,z,t) = T_\infty + \frac{W_{point}}{8(\pi\kappa t)^{3/2}} \exp\left(-\frac{(x-x')^2+(y-y')^2+(z-z')^2}{4\kappa t}\right) \tag{6}$$

where T_∞ is the homogeneous temperature of the medium before the release of the heat pulse. It is important to note that the quantity W_{point} is by itself not an energy, but has the unit K m^3. The local thermal energy density at an arbitrary point in space and time is $C_V(T-T_\infty)$ and the total energy released by the heat pulse (unit: J) at $t=0$ in the point (x',y',z') is obtained by integrating this property over the entire space:

$$\int_{-\infty}^{+\infty}\int_{-\infty}^{+\infty}\int_{-\infty}^{+\infty} C_V[T(x,y,z,t)-T_\infty]\,dx\,dy\,dz = W_{point}C_V \tag{7}$$

Thus relation (6) can be interpreted as the temperature distribution in an infinite medium caused by the heat energy $W_{point}C_V$ released instantaneously at $t=0$ at the point (x',y',z').

In order to find the temperature distribution caused by an instantaneous line heat source, one has to line up many point sources of equal strength $W\,dz'$ along the z-axis, as sketched in the right hand side of Fig. 1. In the infinitesimal limit this means an integration of Eq. (6) over z':

$$T(x,y,z,t) = T_\infty + \frac{W_{point}}{8(\pi\kappa t)^{3/2}}\int_{-\infty}^{+\infty} \exp\left(-\frac{(x-x')^2+(y-y')^2+(z-z')^2}{4\kappa t}\right)dz' \tag{8}$$

With $r^2 = (x-x')^2+(y-y')^2$ denoting the radial distance of a point from the line source, the solution of this integral can be written as

$$T(r,t) = T_\infty + \frac{W_{line}}{4\pi\kappa t}\exp\left(-\frac{r^2}{4\kappa t}\right) \tag{9}$$

Note that now W_{line} has the unit K m^2 and W_{line} C_V is the energy released by the line source per unit length (unit: J m^{-1}).

Next consider the case where the line heat source does not emit an instantaneous heat pulse, but rather generate a constant power over a finite time interval $[0,t]$. In this case relation (9) has to be integrated over t and W_{line} must be replaced by W_{cont} with the dimension [K m^2 s^{-1}]. Correspondingly $W_{cont}(t)C_V$ is the power released by the line heat source per unit length (unit: W m^{-1}). This gives the temperature field at any position r and time t in response to heating by the constant power source over the time interval $[0,t]$:

$$T(r,t) = T_\infty + \frac{W_{cont}}{4\pi\kappa}\int_0^t \frac{\exp\left(-\frac{r^2}{4\kappa(t-t')}\right)}{t-t'}dt' \tag{10}$$

This integral can be solved with the substitution $x = -r^2/4\kappa(t-t')$ to give

$$T(r,t) = T_\infty + \frac{W_{cont}}{4\pi\kappa}\int_x^\infty \frac{\exp(-x)}{x}dx = -\frac{W_{cont}}{4\pi\kappa}Ei\left(-\frac{r^2}{4\kappa t}\right) \tag{11}$$

Here $-Ei(-x)=\int_{x=-r^2/4\kappa t}^{\infty}(\exp(-x)/x)dx$ is the so-called *exponential integral* function.[1]

For the use in thermal conductivity determination from measurements it is convenient to express formula (11) in terms of the (constant) power source $Q=W_{cont}\ C_V$ [W m^{-1}] and the thermal conductivity λ:

$$T(r,t)=T_\infty-\frac{Q}{4\pi\lambda}Ei\left(-\frac{r^2}{4\kappa t}\right) \tag{12}$$

Subsequently the *exponential integral* function is expressed by a series expansion of the form

$$-Ei(-x)=-\gamma-\ln(x)-\sum_{n=1}^{\infty}\frac{(-1)^n x^n}{nn!}=-\gamma-\ln(x)+x-\frac{1}{4}x^2+\cdots \tag{13}$$

where $\gamma=0.577216$ is Euler's constant. For large values of t (small values of x) higher order terms can be neglected and one obtains finally

$$T(r,t)=T_\infty+\left[\frac{Q}{4\pi\lambda}\right]\ln t+\left[\frac{Q}{4\pi\lambda}\left(-\gamma+\ln\frac{4\lambda}{C_V r^2}\right)\right] \tag{14}$$

Since the last term (in brackets) is a constant, it vanishes when Eq. (14) is differentiated after the variable ln$t$:

$$\frac{dT}{d\ln t}=\frac{Q}{4\pi\lambda} \tag{15}$$

This formula provides an easy way to determine the thermal conductivity of a medium by simply measuring the temperature increase of the probe as a function of time in response to a constant heating rate Q. It is usually applied for standard needle probes in homogeneous media with a constant initial temperature or a reasonably small temperature gradient over the domain of interest.

A similar analysis can be performed to obtain the temperature field for heat sources of finite radial extent. A case of practical importance is that of a cylindrical surface source, where a slender cylindrically shaped probe with radius a is considered, which is heated by a constant power Q [W m^{-1}] along the cylinder mantle. In this case the temperature field in the surrounding medium consists of two integral terms:

$$T(r,t)=T_\infty+\frac{Q}{4\pi\lambda}\int_{t'=0}^{t}\frac{1}{(t-t')}\exp\left(-\frac{r^2+a^2}{4\kappa(t-t')}\right)dt' + \frac{Q}{4\pi\lambda}\int_{t'=0}^{t}\frac{1}{(t-t')}\exp\left(-\frac{r^2+a^2}{4\kappa(t-t')}\right)\left[I_0\left(\frac{ra}{2\kappa(t-t')}\right)-1\right]dt' \tag{16}$$

The first integral is similar to that for a constantly heated line source, but modified by the radius a of the cylindrical source. The second term is associated with the cylinder geometry of the sensor. The temperature rise of the heated cylinder mantle is obtained by setting $r=a$ in formula (16). I_0 is the modified Bessel function of the first kind and zeroth order.

In order to judge the importance of the different contributions in real measurements, we have calculated an example using the thermal properties of one of our well characterized test materials (agar), whose thermal properties are the same as those for water. The results for heating the sensor with a power of $Q=6$ W/m over a period of 10^5 s are displayed in Fig. 2 as a semi-logarithmic plot. The full line represents the complete solution calculated with formula (16) for $r=a$, while the dashed and dashed–dotted lines show the contribution of the first and the second term, respectively. As can be seen, at heating times $t>10^2$ s the cylindrical surface source term approaches a constant value, while the line source term shows a linear increase on a semi-logarithmic scale, with an inclination very similar to that of the full solution. Because of this fact the standard evaluation approach for a line heat source sensor can also be used for a large hollow cylindrical sensor like the LNP01 shown in Fig. 4, provided measurement time is long enough.

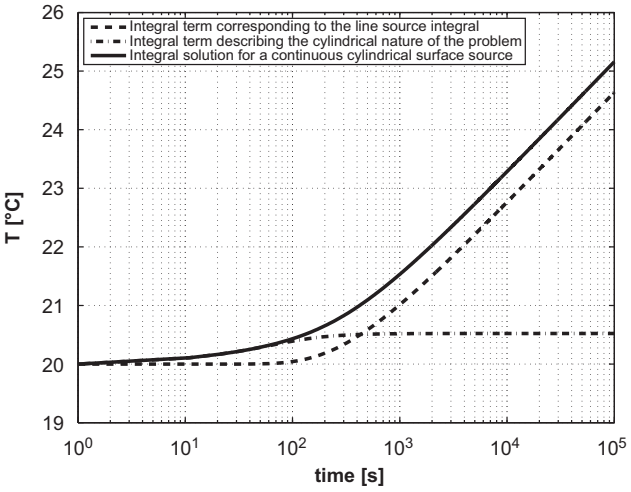

Fig. 2. Influence of the finite diameter of a hollow cylindrical sensor on the temperature response due to heating with a constant power.

3.2. Formulae with thermal resistance and non-ideal sensor properties

The formulae presented up to now are idealized in the way that they do not include any thermal properties of the sensor itself, since they assume that the heat source is concentrated either in a line or along the mantle of a cylinder. However, for real sensors this is not true. Even when one remains with the approximation of a long and thin axisymmetric sensor, the heated sensor occupies a finite volume (per unit length) and thus has its own characteristic thermal properties, which usually differ from the properties of the surrounding medium. Moreover, in the case of a cylindrical sensor with finite radius a there may also exist a thermal resistance across the boundary between sensor and surrounding material, which causes a temperature discontinuity.

In the following we compile the most useful formulae which include a finite thermal surface conductance H (unit: W m^{-2} K^{-1})[2] and a non-negligible sensor heat capacity S (unit: J m^{-1} K^{-1}). Note that S is the specific volumetric heat capacity of the sensor material multiplied with the sensor cross section. Thus it is not a true material property, but is also depends on the sensor's geometry and size.

For a simple representation of the relevant formulae it is convenient to define three dimensionless variables involving all basic parameters of the problem (Jaeger, 1956):

$$\tau=\frac{\lambda t}{C_V a^2}=\frac{\kappa t}{a^2} \tag{17}$$

$$\alpha=\frac{2\pi a^2 C_V}{S} \tag{18}$$

$$h=\frac{\lambda}{aH} \tag{19}$$

[1] A suitable reference to look up the analytical representation of the integrals and the various Bessel functions frequently occurring in this review is the *Handbook of Mathematical Functions* edited by Abramovich and Stegun (1972).

[2] Thermal conductance and thermal resistance are defined analogous to their counterparts in the theory of electricity. Thermal resistance is the inverse of thermal conductance H. Thus $H\to\infty$ is equivalent to $(1/H)\to 0$, i.e. there is no temperature discontinuity across the respective boundary (Incropera et al., 2007).

τ can be considered as a *dimensionless time* and is also called the *Fourier number*. It represents the characteristic time for the propagation of the heat wave in the medium surrounding the heated cylinder with radius a. α is 2 times the ratio of the heat capacity of the sensor to the heat capacity of an equivalent volume consisting of the surrounding material. Finally the parameter h is proportional to the thermal resistance between sensor and surrounding medium.

First consider again an instantaneous cylindrical heat source. This is equivalent to the case that the cylindrical sensor is initially at a higher temperature than the surrounding medium, and that this temperature disequilibrium is relaxed over time by heat conduction across the thermal resistance $1/H$ between sensor and medium. In formula (20) given below T_0 is the initial sensor temperature while T_∞ is the initial temperature of the surrounding medium. Moreover it is assumed that the thermal conductivity of the sensor material is very high compared to that of the surrounding material ($\lambda_{sensor}\to\infty$) so that the sensor as a whole can always be considered as isothermal, while its temperature adapts to that of the surroundings. With these approximations one obtains

$$T(\tau)=T_\infty+(T_0-T_\infty)\frac{4\alpha}{\pi^2}\int_0^\infty\frac{\exp(-\tau x^2)\,dx}{xf(x)} \tag{20}$$

$$f(x)=[xJ_0(x)-(\alpha-hx^2)J_1(x)]^2+[xY_0(x)-(\alpha-hx^2)Y_1(x)]^2 \tag{21}$$

Again, Bessel functions appear in the solutions. J_0 and J_1 are the regular Bessel functions of the first kind and order zero and one, while Y_0 and Y_1 are the Bessel functions of the second kind and order zero and one. Note that these functions are different from the type $I_0(x)$ appearing in formula (16), where the *modified* Bessel function of zeroth order appears. A generalization of this case is discussed further in the Appendix.

For the case of a cylinder which is initially at the same temperature as the surrounding medium and heated for a finite time interval with a constant power Q (unit: W m^{-1}), one obtains the following formula for the temperature increase of the sensor as a function of time (Jaeger, 1956):

$$T(\tau)=T_\infty+\frac{2Q\alpha^2}{\lambda\pi^3}\int_0^\infty\frac{[1-\exp(-\tau x^2)]\,dx}{x^3f(x)} \tag{22}$$

$$f(x)=[xJ_0(x)-(\alpha-hx^2)J_1(x)]^2+[xY_0(x)-(\alpha-hx^2)Y_1(x)]^2 \tag{23}$$

Here again the assumption was made that the thermal conductivity of the sensor is large compared to that of the surroundings.

Another case of interest for the development of thermal conductivity sensors is obtained when two concentric cylinders are surrounded by an infinite medium. This configuration resembles an electrically heated cable insulated by a thin electrically isolating sheath, which is surrounded by soil. For such a geometry closed solutions with a similar structure as the formulae given above can also be found. They have been explicitly worked out in the paper by Jaeger (1956).

3.3. Axisymmetric configurations with finite length

Analytic solutions for heat conduction problems in cylindrical geometry can also be found for the case that the temperature field depends not only on r and t, but also on the vertical coordinate z and the azimuth φ. Solutions to this problem are given by Banaskiewicz (2002a–e) and Woodfield et al. (2008) for different boundary conditions.

For the theory of heat conductivity sensors, the inclusion of a z-dependence is of particular interest, because this allows to treat arbitrary axisymmetric configurations (including such ones where the diameter over length ratio is not small) in a more rigorous way. The central mathematical tools to treat such problems are the *Laplace transformation* and the *Green function* (Courant and Hilbert, 1962; Bayin, 2006). However, the disadvantage of following this analytic approach is that formulae become extremely lengthly and cumbersome to derive whenever one goes beyond a pure (r,t) dependence. Therefore, we cannot give a fully comprehensive description of the multi-dimensional problem and its solution in the frame of this review, but rather refer to the original sources (Carslaw and Jaeger, 1959; Jaeger, 1941) and to the above mentioned papers by Woodfield et al. (2008) and by Banaszkiewicz (2002a–e). In this subsection we just illustrate the fundamental ideas underlying the solution of the axisymmetric z-dependent problem by means of a Green function, which would be applicable to many of the sensor designs shown in the subsequent section.

Consider a two-component system consisting of a hollow cylindrical sensor (Domain 1) with an inner diameter a, an outer diameter b and a finite length L, as sketched in Fig. 3. The surrounding medium (Domain 2) extends from the outer sensor radius b to an arbitrary radius c, whereby typically $c\gg b$, with the limiting case $c\to\infty$ being also possible. The quantities referring to the cylindrical sensor and the surrounding medium are marked by the respective domain subscripts 1 and 2 e.g. $T_1(r,z)$ or $T_2(r,z)$. We use $T(r,z)$ to denote $T_1(r,z)$ and/or $T_2(r,z)$ when expressing properties which hold for both domains. Similarly κ and λ may represent κ_n and λ_n with $n=1$ and/or $n=2$, respectively.

In the relatively simple case illustrated here the whole extension of the z-domain is limited to the length L of the sensor, so that appropriate boundary conditions have to be specified both at these z-levels over the radial interval $a<r<c$, and at $r=a$ and $r=c$ over the vertical interval $0<z<L$.

The heat conduction equations for the sensor and the medium domain can then be written in the form

$$\frac{\partial T_n}{\partial t}-\nabla\cdot(\kappa_n\nabla T_n)=0\quad(n=1,2) \tag{24}$$

Eqs. (24) imply that there is no heat production in the interior of the domains. Any heat is generated at the boundaries and enters the domains via conduction. Let S_a be the inner cylindrical boundary of the sensor defined by $r=a$, $0\le z\le L$. Similarly, S_b denotes the boundary between the sensor and the surrounding medium ($r=b$), and S_c the outer boundary at $r=c$. Furthermore, let

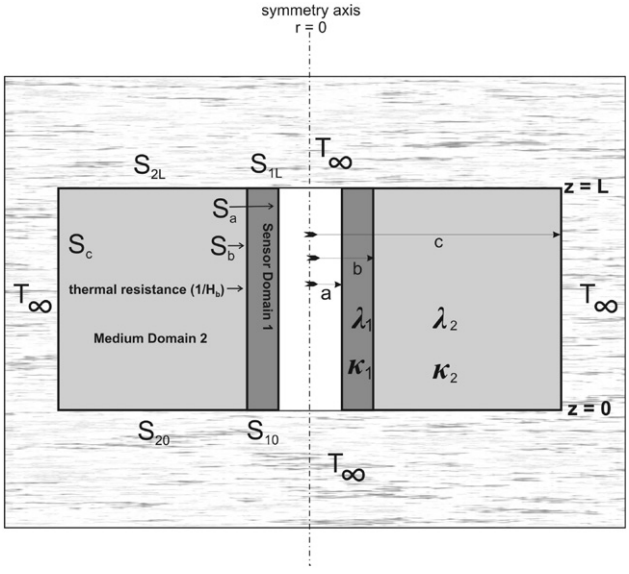

Fig. 3. Sketch of the axisymmetric heat conduction model with finite length.

S_{n0} and S_{nL} be the lower and upper disc bordering the domains n; e.g. S_{10} is defined by $a \le r \le b$ and $z=0$, S_{2L} by $b \le r \le c$ and $z=L$. The boundaries S_a, S_{n0} and S_{nL} ($n=1,2$) can be specified by the following rather general boundary conditions:

$$\Phi(r,z) = \lambda \frac{\partial T}{\partial n} + H(T - T_\infty) \tag{25}$$

The surface power sources Φ are generated per area in the respective boundaries, dissipating into Domain 1 or Domain 2 and into the environment outside the Domains 1 and 2 (the environment is assumed to be at temperature T_∞). H is the surface conductance and may vary over the boundaries, which are again specified by their respective indices. $\partial T/\partial n$ signifies the derivative of T with regard to the outward pointing surface normal. In terms of r and z we get the following more specific notation for the different boundaries:

$$S_{10}(a<r<b, z=0): \quad \Phi_{10} = -\lambda_1 \frac{\partial T_1}{\partial z} + H_{10}(T_1 - T_\infty) \tag{26}$$

$$S_{20}(b<r<c, z=0): \quad \Phi_{20} = -\lambda_2 \frac{\partial T_2}{\partial z} + H_{20}(T_2 - T_\infty) \tag{27}$$

$$S_{1L}(a<r<b, z=L): \quad \Phi_{1L} = +\lambda_1 \frac{\partial T_1}{\partial z} + H_{1L}(T_1 - T_\infty) \tag{28}$$

$$S_{2L}(b<r<c, z=L): \quad \Phi_{2L} = +\lambda_2 \frac{\partial T_2}{\partial z} + H_{2L}(T_2 - T_\infty) \tag{29}$$

$$S_a\ (r=a, 0<z<L): \quad \Phi_a = -\lambda_1 \frac{\partial T_1}{\partial r} + H_a(T_1 - T_\infty) \tag{30}$$

At the outer boundary of Domain 2 (along $r=c$) we define

$$S_c\ (r=c, 0<z<L): \quad T_2 = T_\infty \tag{31}$$

which means that the temperature is not influenced by sensor heating. Therefore, the temperature T_∞ of the environment is assumed to be a constant value, which does not vary with time. The boundary conditions (26)–(30) are the so-called *radiation boundary conditions* (Carslaw and Jaeger, 1959, p. 19). In particular Φ_a describes the heat supply (unit: W m^{-2}) to the inner mantle of the sensor tube and can be re-written as $Q_a = 2\pi a \Phi_a$ to give the heat supply per unit length (in W m^{-1}). The upper and lower boundaries could be either open to empty space and receive radiation from outside or composed of other layers of material with specified material and contact parameters, which finally determine the heat flow from and to the interior.

An important interior boundary is the interface between sensor and medium ($r=b, 0<z<L$), where a thermal resistance ($1/H$) can be defined, implying the following interface conditions:

$$\lambda_1 \left[\frac{\partial T_1}{\partial r}\right] = \lambda_2 \left[\frac{\partial T_2}{\partial r}\right] \tag{32}$$

$$-\lambda_2 \frac{\partial T_2}{\partial r} = H_b(T_1 - T_2) \tag{33}$$

Finally initial conditions for the sensor and the surrounding material temperature must be defined, which can be arbitrary functions of r and z:

$$T(r,z,t=0) = f(r,z) \quad (a \le r \le b, 0 \le z \le L) \tag{34}$$

The above definitions specify the problem completely. To obtain a solution for the temperature evolution in the Domains 1 and 2 in terms of the power Φ supplied at the boundaries, one utilizes the Green function $G(r,z,r',z',t-t')$, which is a solution of the inhomogeneous heat conduction equation

$$-\frac{\partial G}{\partial t'} - \nabla' \cdot (\kappa \nabla' T) = \delta(r-r')\delta(z-z')\delta(t-t') \tag{35}$$

throughout the Domains 1 and 2, satisfying homogeneous boundary conditions (the boundary conditions (26)–(31) with vanishing Φ terms and $T_\infty = 0$) and the initial condition (at $(t-t')=0$):

$$G(r,z,r',z';0) = \delta(r-r')\delta(z-z') \tag{36}$$

Note how the Green function depends on the space and time coordinates: (r,z,t) are the particular position and time of observation for which the temperature should be determined, while (r',z',t') are source location and time acting as integration variables in the final formulae for the temperature $T(r,z,t)$. Once the Green function G in the medium and the sensor has been determined, solutions for the temperature field as a function of time and space variables can be calculated in terms of the initial temperature field $f(r',z')$ and the surface power sources Φ supplied to the boundaries. If the specific heat of the sensor and the surrounding medium is the same, the following analytic expression for the time and space dependent temperature field is obtained:

$$\begin{aligned} T(r,z,t) = T_\infty &+ \int_0^L \int_a^c G(r,z,r',z',t)(f(r',z') - T_\infty) 2\pi r'\, dr'\, dz' \\ &+ \int_0^t \int_a^b \frac{\kappa_1}{H_{10}} \Phi_{10}(r',t') \frac{\partial G}{\partial z'}(r,z,r',0,t-t') 2\pi r'\, dr'\, dt' \\ &+ \int_0^t \int_b^c \frac{\kappa_2}{H_{20}} \Phi_{20}(r',t') \frac{\partial G}{\partial z'}(r,z,r',0,t-t') 2\pi r'\, dr'\, dt' \\ &- \int_0^t \int_a^b \frac{\kappa_1}{H_{1L}} \Phi_{1L}(r',t') \frac{\partial G}{\partial z'}(r,z,r',L,t-t') 2\pi r'\, dr'\, dt' \\ &- \int_0^t \int_b^c \frac{\kappa_2}{H_{2L}} \Phi_{2L}(r',t') \frac{\partial G}{\partial z'}(r,z,r',L,t-t') 2\pi r'\, dr'\, dt' \\ &+ \int_0^t \int_0^L \frac{\kappa_1}{H_a} \Phi_a(z',t') \frac{\partial G}{\partial r'}(r,z,a,z',t-t') 2\pi a\, dz'\, dt' \\ &- \int_0^t \int_0^L \kappa_2 T_\infty \frac{\partial G}{\partial r'}(r,z,c,z',t-t') 2\pi a\, dz'\, dt' \end{aligned} \tag{37}$$

The derivation can be accomplished in analogy to the procedure described in Chapter 14 of Carslaw and Jaeger (1959). As a result of a lengthy calculation, the Green functions of the problem are expressed as a sum of terms which decay exponentially in time with r- and z-dependent coefficients expressed by Bessel functions. More details can be found in Banaszkiewicz (2002a) for the present case, and in Carslaw and Jaeger (1959) for several other boundary conditions. In case of $c=\infty$ the sum degenerates into an integral. The summation will inevitably involve truncation errors when it is aborted at some finite number of terms. While in principle always an arbitrarily accurate solution can be obtained, the influence of the truncation errors (which typically lead to nonphysical oscillations in the vicinity of temperature discontinuities) needs to be carefully investigated in any practical application.

In principle, a similar algorithm can be used to calculate solutions for composite regions consisting of horizontal layers with finite vertical extent, between which the thermal properties may vary and additional thermal resistances may exist. In this case the upper and lower boundary conditions of the problem described above would become interface conditions similar to the boundary b, which connect different sublayers (Banaszkiewicz, 2002d).

4. Probes for geophysical and planetary applications

4.1. Laboratory prototypes

As already pointed out above, the most simple way to evaluate the thermal conductivity of a solid and/or porous material is to insert a long and thin needle sensor into a reasonably large sample and to measure the temperature increase in response to

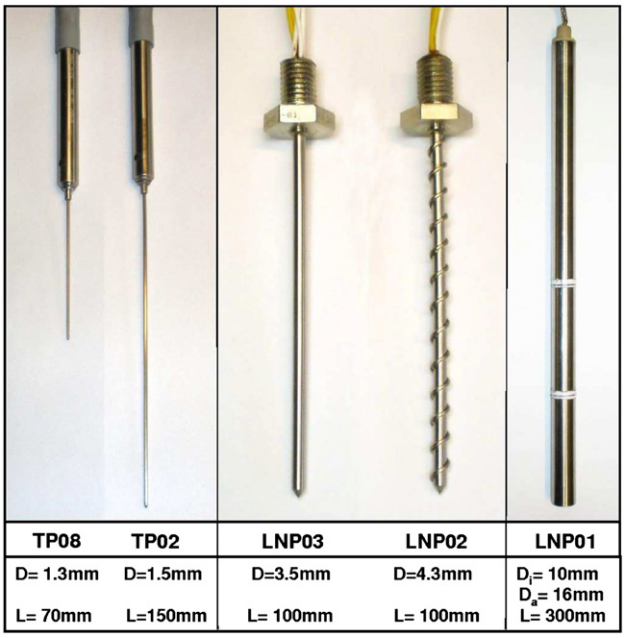

Fig. 4. Thermal conductivity sensors from Hukseflux. Left: commercial needle sensors; middle: custom-made more robust needle sensors; right: hollow cylindrical sensor.

a controlled heating rate over a large part of its length (see e.g. Wechsler, 1992). As long as the measured materials are reasonably homogeneous over the length of the sensor, thermal conductivity can be determined by using the formulae for an infinitely long line heat source. Typical examples for such types of sensors are the models TP02 or TP08 from the company *Hukseflux* (Fig. 4, left). They have a very favorable length over diameter ratio, which reduces measurement errors to $<3\%$.[3]

This can, however, only be achieved by using thermocouples for the temperature measurement, because they can be installed inside a very narrow volume. The disadvantage of such commercial sensors is, however, that they are mechanically weak, which can cause a problem in field or space applications. Alternative versions with a somewhat worse length over diameter ratio, but a much higher mechanical robustness, are the custom-made sensors LNP02 and LNP03, with a length of 100 mm and a diameter of 3.5 mm (Fig. 4, middle). Models LNP02 and LNP03 are identical except of the outer shape. LNP02 has the shape of an auger drill and thus could be used as a component in a combined drilling and thermal conductivity measurement system. In order to check if the screw-like winding on the LNP02 as compared with the smooth surface of the LNP03 has any influence on the thermal conductivity measurement, we compared measurement results from both sensors in the same materials, but could not find any significant difference of the measurement values. However, it must also be noted that these sensors, due to their less favorable length over diameter ratio, need to be calibrated, best by using a TP02 in the same materials and under identical environmental conditions.

Another type of sensor that is sometimes used in field and possibly in future space applications are thicker hollow cylinders as the model LNP01 (Fig. 4, right). Extensive tests on the performance of such a sensor both in air and in low pressure conditions have recently been performed by Hütter (2011). Aside of its robustness, the advantage of such a sensor type is that it is suitable for measurements in coarse-grained granular material with grain sizes up to several centimeters (Kömle et al., 2008, 2010). Again, when using the standard evaluation method to derive thermal conductivity from the temperature curve, calibration measurements are necessary in advance.

A typical example for the evaluation of a line heat source measurement in a medium with a small temperature gradient is shown in Fig. 5. It stems from a measurement in frozen agar (which should have the same thermal conductivity as regular water ice) and is discussed in more detail in Kömle et al. (2008). The upper left panel shows the raw data measured by the thermocouple positioned in the heated part of the needle sensor Huksefux TP02. Heating starts after 1/2 of the measurement interval has elapsed. If the temperature distribution in the sample is not fully equilibrated at the beginning of the heating period, the temperature data can be corrected by extrapolating the trend into the heating interval and subtracting it from the measured temperature (upper right panel). This results in a corrected temperature profile (lower left panel). On this corrected plot the suitable part for thermal conductivity determination (linear temperature increase versus $\ln t$) has to be identified and data points are fitted by a linear regression line, which provides the inclination of the curve. Using this value, formula (15) is applied to calculate λ.

However, when using the evaluation method outlined above for determining the thermal conductivity of a material, one always has to check in advance if the conditions for its applicability are fulfilled. Aside of the thermal diffusivity κ of the sample to be measured, the geometric dimensions of sensor and sample are the key parameters. There are two characteristic times that should be estimated in advance, when performing such measurements. First, there is a transient time, where the sensor undergoes self-heating and thus the temperature increase as a function of time is strongly influenced by the sensor properties. For the standard evaluation procedure this time interval should not be used for thermal conductivity determination. It can be estimated as (Vos, 1955)

$$t_{trans} = \frac{50a^2}{4\kappa} \tag{38}$$

where a is the radius of the probe and κ the thermal diffusivity of the surrounding material. Strictly this formula applies to a full cylinder with radius a. To describe the case of a hollow cylinder with inner and outer radii a_1 and a_2 one should define an equivalent radius

$$a_e = \sqrt{(a_2^2 - a_1^2)} \tag{39}$$

with the same cross section as the hollow tube and use it instead of a in formula (38).

The upper limit of the measurement interval useable for data evaluation is typically caused by the finite dimension of the sample (this applies primarily to laboratory measurements with samples of finite size, while for field measurements it is hardly relevant). The reason for the existence of this upper limit is that the heat wave might reach the boundary of the sample container and thus the boundary conditions there begin to influence the temperature profile in a way not included in the theory. The heat wave may be reflected from the boundaries or other properties of the environment can influence the solution.

An estimate for this maximum measurement time is given by the formula (Goodhew and Griffiths, 2004; Vos, 1955):

$$t_{max} = \frac{0.6(r_{sample} - a)^2}{4\kappa} \tag{40}$$

[3] Favorable length over diameter ratios have been defined by the *American Society for Testing and Materials* (ASTM) under numbers D9530-01 and 5334-00. They specify that commercial thermal conductivity measurement needles should have a length-over-diameter ratio of greater than 20 to fulfill the standards (see, for example the websites www.thermal.decagon.com or www.hukseflux.com.

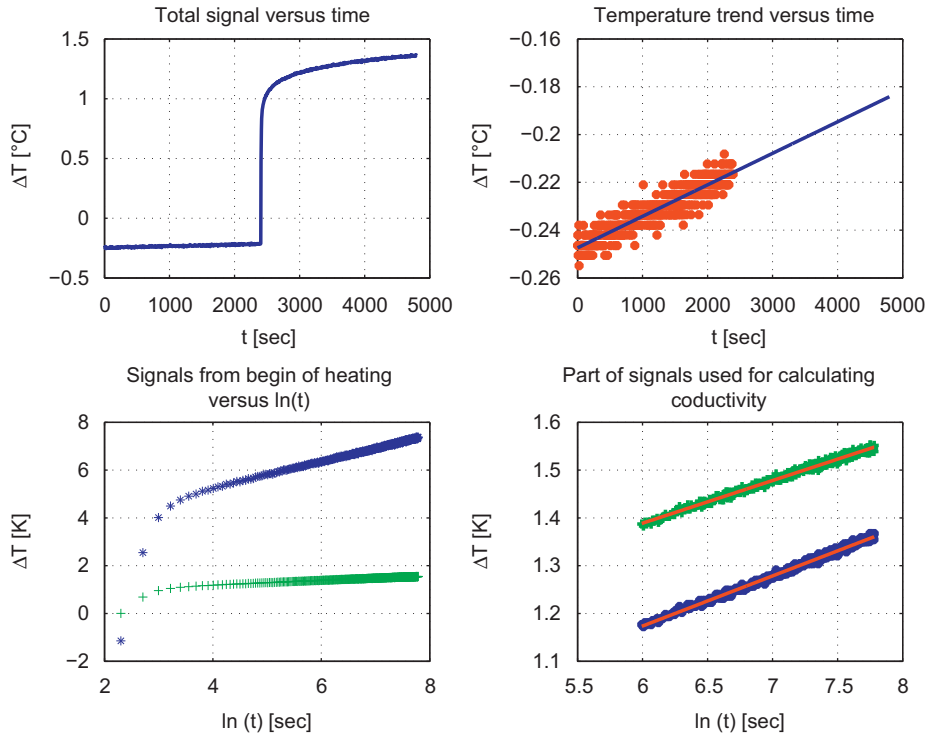

Fig. 5. Standard evaluation procedure for a thermal conductivity measurement with a heated needle sensor (after Kömle et al., 2007).

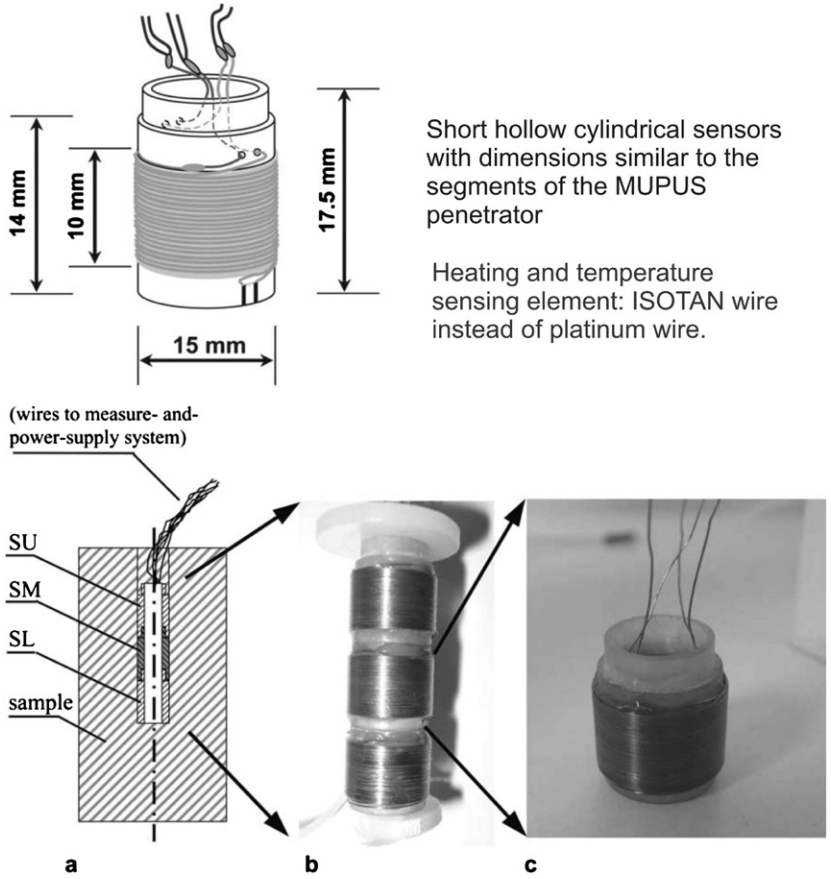

Fig. 6. Short cylindrical thermal conductivity sensors for future space applications constructed and tested at the Space Research Centre, Warsaw, Poland. The sensors are similar in size as the individual segments of the MUPUS probe (after Banaszkiewicz et al., 2007).

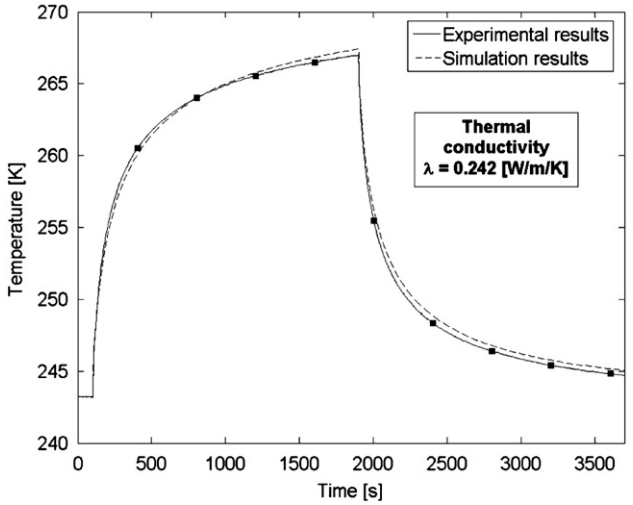

Fig. 7. Temperature measurement during one heating cycle in a powder sample composed of a mixture of olivin and gabbro minerals (after Banaszkiewicz et al., 2007).

In order to study in more detail, how short cylindrical heaters can be reliably used as thermal conductivity sensors, Banaszkiewicz et al. (2007) have constructed an assembly of three identical sensors with a diameter of 15 mm and a heated length of 10 mm each. They were stacked together axially to form a compact unit as shown in Fig. 6.

These miniature sensors use separate electrical circuits for heating and temperature sensing, similar as the prototypes described above. For temperature sensing a thin (75 μm diameter) platinum wire was used, connected to the measurement electronics in a 4-wire technique. The dependence of the electrical resistance of the platinum on temperature is very well known and almost linear over a large temperature range. On the other hand, as a heater element a 200 μm diameter ISOTAN wire was used, whose electrical resistance is very little temperature dependent and therefore provides a constant and stable heating power when connected to a constant voltage source. Both wires are electrically insulated and wound around a hollow cylindrical tube made of fiberglass, as shown in Fig. 6.

Sensors of that kind are easy to manufacture and assure close to constant heating power and high accuracy of temperature determination. A numerical model has been used for determination of heat conductivity of different materials in previous investigations (Banaszkiewicz et al., 2007). A typical plot comparing measurement results with a fit by a numerical model is shown in Fig. 7. These sensors are small and relatively flat, which is an advantage in case of using them as a main or "piggy-back" payload for different kinds of low velocity penetrators being considered for future space missions. An example is the CHOMIK device for the Phobos-Grunt mission to the Mars satellite Phobos (Grygorczuk et al., 2010).

4.2. Bullard probe for terrestrial applications

One of the first instruments for measuring the heat flux from the Earth's interior was the probe constructed and used by Bullard (1954). It was essentially a hollow steel tube of 27 mm outer diameter and 4.72 m length, attached to an electronics and recording box at its top side. A photo of the apparatus is shown in Fig. 8. Bullard's basic goal was the measurement of the heat flux from the Earth's interior. After having done measurements in deep boreholes drilled into the continental crust, he tried to measure the heat flux from the floor of the Atlantic Ocean at several sites, having in mind the idea that in this case external influences (diurnal and annual heat waves caused by periodic solar irradiation) should be negligible. To perform the measurements, the probe was let down towards the seafloor in a controlled way by a winch and allowed to penetrate the seafloor sediments with a speed of about 3 m s^{-1}. This was in most cases enough to let the probe penetrate into the ocean floor over its full length of more than 4 m. The temperature gradient over these uppermost 4 m was then determined by recording the temperature readings of the two thermocouples installed close to the upper and lower end of the probe, which had an axial distance of 4.58 m from each other. Usually for a single run the probe stayed in the soil of the ocean floor for about 30 min. After this time it was withdrawn and pulled back to the surface by the winch.

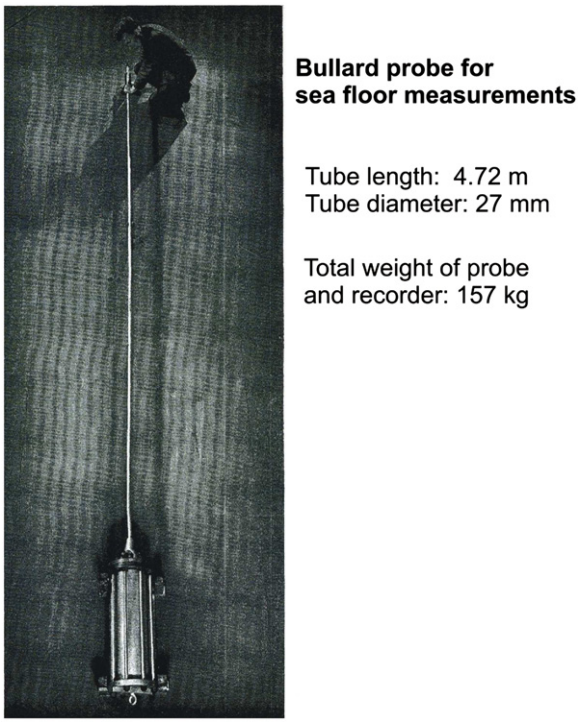

Fig. 8. Bullard's probe for measuring the terrestrial heat flow in deep sea regions of the Atlantic Ocean (after Bullard, 1954).

Naturally, in such an experiment some heat will be generated during penetration of the probe into the sea floor until it comes to rest in a stable position. This will cause the probe to be initially warmer than the natural environment. The decline of the probe temperature towards the undisturbed condition can be calculated by using the axisymmetric solution for the decay of a heat pulse as given by formulae (20)–(21).

In the case of Bullard's measurements at the seafloor one can expect that the thermal contact between probe and medium was very good. Thus one could safely assume that $h=0$ and the integral (20) can be evaluated with only α and τ as parameters. However, for measurements in boreholes (especially when the environmental gas pressure is low) h has a finite value and cannot be neglected. We will discuss this case in more detail in the next section.

4.3. Lunar thermal probes on the Apollo missions

The measurements of thermal conductivity and heat flux on the Moon, performed in the frame of the manned Apollo missions 15 and 17, were the first extraterrestrial *in situ* heat flux and thermal conductivity experiments performed in the history of

space research. The measurements were performed at two lunar sites, namely near the Hadley Rille by *Apollo 15* and in the Taurus–Littrow site by the *Apollo 17* team. In this section we review the technical build-up and the operation of the heat flux and conductivity probes used and some of the results obtained. Fig. 9 shows the general setup of the heat flow experiment. Two

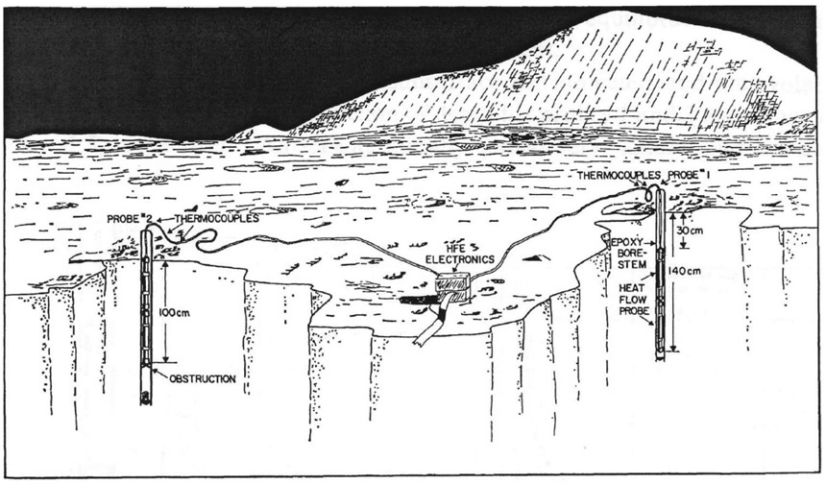

Fig. 9. Setup of the lunar heat flux and thermal conductivity experiment performed on the *Apollo 15* and *17* missions (after Langseth et al., 1972c).

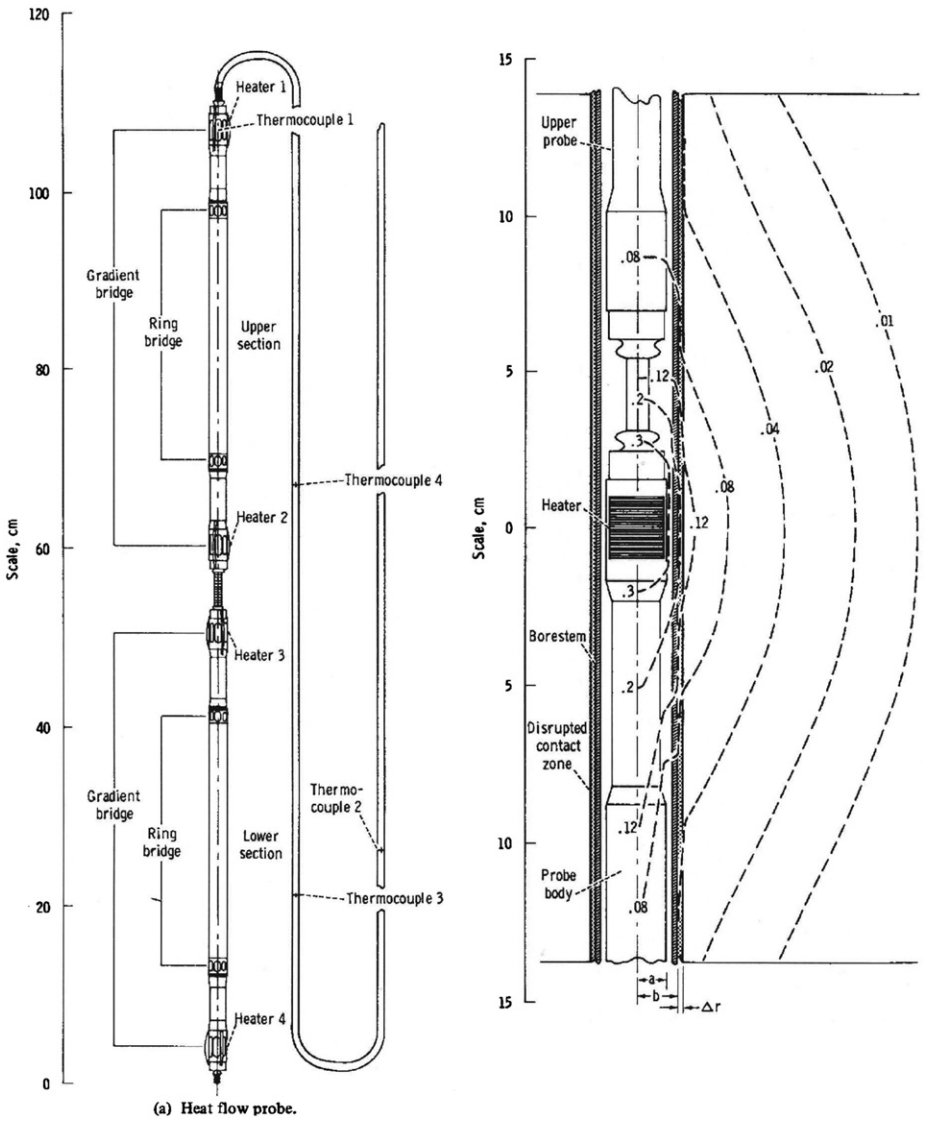

Fig. 10. The Apollo lunar heat flux and conductivity probe (after Langseth et al., 1972b).

identical probes were used, which were placed within about 10 m distance on the lunar surface and operated by a common electronics. Both for *Apollo 15* and the analogous experiment on *Apollo 17* the setup and the evaluation procedures are well described in the preliminary science reports published as NASA Special Publications (Langseth et al., 1972a, 1972b, 1972c). Also the respective articles in the *Lunar Sourcebook* (Heiken et al., 1991) should be mentioned here. Furthermore, all procedures related to the experiments conducted by the astronauts during their stay at the lunar surface are documented in great detail by Sullivan (1994). The construction was designed to determine both the undisturbed heat flux from the interior and the heat conductivity in different depths. The performance of the experiment consisted of two major steps: (i) A hand-held drill consisting of a borestem and a drillhead was used to prepare a drill hole in the lunar regolith, designed for a maximum depth of 3 m (this depth was never reached in any of the four holes drilled for these tests, the maximum insertion depth actually reached at one of the two boreholes at the *Apollo 17* site was 2.54 m). After drilling was completed down to the depth that was possible, the borestem (a tube made of epoxy material) was left inside the drillhole in order to stabilize it and for the measurements the heat flow probes were inserted into this tube. The structure and dimension of the heat flow probes is shown in more detail in Fig. 10. They consisted of two 50 cm long segments screwed together and equipped with heaters and thermocouples as shown in the figure.

It is worthwhile to reconsider the procedure used by Langseth et al. to evaluate both the thermal conductivity of the subsurface layers and the undisturbed heat flux from the interior. Generally, they followed a similar evaluation procedure to find the interior heat flux as Bullard (1954) used for his seafloor measurements. However, the situation is much more complicated in this case, because of several facts:

- For determining the local heat conductivity of the surrounding material active heaters close to the ends of the individual segments were used. However, the shape of the heaters was not that of a long thin needle but rather that of a short cylindrical tube. Therefore, determination of thermal conductivity of the surrounding material in terms of the standard theory (heated thin needle) is at least not straightforward.
- Although the overall geometry was still axisymmetric, there exist non-negligible thermal resistances, that have to be taken into account. One is the resistance between the inserted probe and the borestem which acts as the casing for the former, and the second resistance occurs between the outer wall of the borestem and the regolith.

To take the additional thermal resistances into account, the formulae for buried cables of finite diameter given by Jaeger (1956) have to be extended in such a way that there is also a finite thermal resistance between the outer concentric cylinder and the surrounding soil. In this particular problem the inner cylinder is the heat flow probe with contact conductance H_1 to the borestem and the outer concentric cylinder is the borestem with contact conductance H_2 to the surrounding undisturbed regolith. Assuming that the temperature of the regolith is T_∞ and the temperature of the borestem at the time of insertion into the borehole is T_0 (usually $T_0 > T_\infty$ because borestem and probes were stored in a box that was considerably warmer than the ground temperature)—the decay of the probe temperature (inner cylinder) towards an equilibrium with the ground temperature can be described by the following integral formula:

$$T(\tau) = T_\infty + (T_0 - T_\infty)\frac{4\alpha}{\pi^2}\int_0^\infty \frac{(1-Ax^2)\exp(-\tau x^2)\,dx}{x f(x)} \tag{41}$$

$$f(x) = [x(1-Ax^2)J_0(x) + [hx^2(1-Ax^2) - \alpha(1-Bx^2)]J_1(u)]^2 + [x(1-Ax^2)Y_0(x) + [hx^2(1-Ax^2) - \alpha(1-Bx^2)]Y_1(x)]^2 \tag{42}$$

To evaluate the integral, dimensionless auxiliary variables analogous to relations (17)–(19) have to be calculated:

$$\tau = \frac{\kappa t}{b^2} \tag{43}$$

$$\alpha = \frac{2\pi b^2 \varrho c}{S_1 + S_2} \tag{44}$$

$$h = \frac{\lambda}{bH_2} \tag{45}$$

$$\gamma = \frac{S_1}{2\pi a H_1} \tag{46}$$

$$A = \frac{\gamma\kappa}{b^2}\frac{S_2}{(S_1+S_2)} \tag{47}$$

$$B = \frac{\gamma\kappa}{b^2} \tag{48}$$

The parameters needed to calculate the above expressions are listed in Table 1. We note that in the *Preliminary Science Report* for the Heat Flow Experiment on *Apollo 15* Langseth et al. (1972a) have already given a solution of this problem. However, it appears that his formula is not completely correct and contains at least printing errors, which might lead to wrong results when the formula is applied to similar problems in the future. Therefore, we have re-analyzed the problem from the beginning on the basis of Carslaw and Jaeger's theory and obtained as a result formulae (41) and (42) as given above. The most important steps of this re-calculation are documented in the Appendix.

This allows to calculate the decay of the probe temperature towards an equilibrium temperature (that of the surrounding material) with time. Extrapolation to the equilibrium case is a pre-requisite for being able to determine the natural (undisturbed) temperature gradient, which is needed to calculate the interior heat flux. Ideally, a situation close to equilibrium should be reached before starting active heater experiments for thermal conductivity determination. Due to the long time scales in the poorly conducting regolith of the Moon, full adaption of the probe temperature to that of the surrounding soil was not reached, gentle cooling was observed even several weeks after the insertion of the probes. This issue was also addressed by Grott et al. (2010) in their recent re-analysis of the Apollo thermal measurement results.

From Fig. 10 one can easily see that the geometry of the heaters is far from that of a slender line heat source, which would allow simple determination of the thermal conductivity of the surrounding soil. How did the authors handle this problem? They argued that it should be possible to use nevertheless a similar relation for the temperature increase with time as it is known for the line heat source, namely

$$\Delta T = C_1 \ln t + C_2 \tag{49}$$

where the constants C_1 and C_2 depend in principle both on the thermal parameters of the media (probe and surrounding material) and on the contact properties (thermal conductance or resistance, respectively) between soil and probe. In practice it turned out that the rear parts of the measured temperature profiles (the ones that would typically be used when applying the standard line heat source method) indeed could be well fitted by a function of the form (49) and could also be well reproduced by a more complete finite difference model. Some measured temperature profiles from the active thermal conductivity

Table 1
Input parameters for calculating the temperature equilibration of an initially warmer probe in an infinite medium—model for the Apollo heat flow probes.

Symbol	Units	Description
		Parameters of the surrounding material
ϱ	kg m^{-3}	Density of the surrounding material, *can be estimated from supplementary measurements* (*returned samples*)
C_M	J kg^{-1} K^{-1}	Heat capacity (per unit mass) of the surrounding material from this $C_V = \varrho C_M$, can be calculated *can be estimated from supplementary measurements* (*returned samples*)
λ	W m^{-1} K^{-1}	Thermal conductivity of the surrounding material, **unknown parameter to be determined from measurement**
		Parameters of the instrument (probe and borestem)
a	m	Radius of the inner cylinder (heat flow probe)
b	m	Radius of the outer cylinder (bore stem)
S_1	J m^{-1} K^{-1}	Heat capacity per unit length of the inner cylinder, *can be determined by lab test in advance*
S_2	J m^{-1} K^{-1}	Heat capacity per unit length of the outer cylinder, *can be determined by lab test in advance*
H_1	W m^{-2} K^{-1}	Thermal conductance between inner and outer cylinder, *can be determined by lab test in vacuum conditions in advance*
		Parameters involving probe and target properties
H_2	W m^{-2} K^{-1}	Thermal conductance between outer cylinder and surrounding material, **unknown parameter to be determined from measurement**

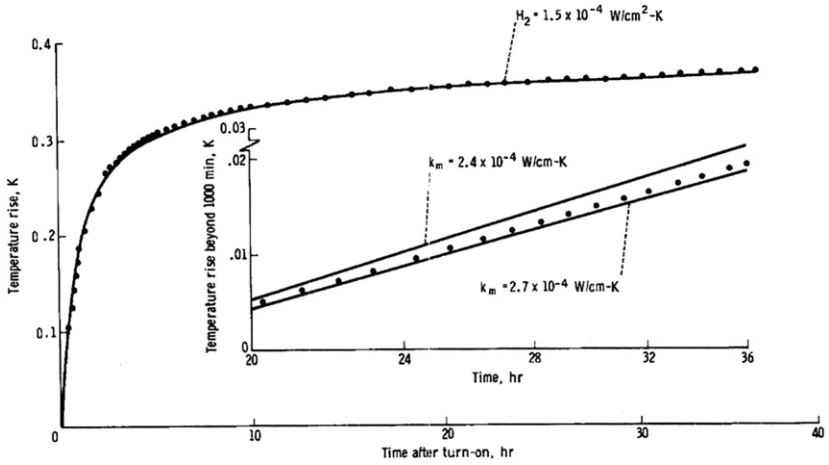

Fig. 11. Evaluation procedure and results from the Apollo heat flux and thermal conductivity experiment (after Langseth et al., 1972b).

measurement at the *Apollo 15* site are shown in Fig. 11. A possible explanation for this surprisingly good coincidence (also put forward by the authors) is that—although the heaters themselves are short—the high thermal resistance between borestem and surroundings and the good thermal conductivity of the borestem as compared to the surrounding regolith causes a close to isothermal temperature distribution over a reasonably long part of the borestem. This is almost equivalent to homogeneous heating over a longer part of the borestem.

Since most of the parameters listed in Table 1 can be well constrained, there remain two major unknowns: the thermal conductivity of the surrounding material λ and the contact conductance between material and probe H_2. λ can be determined independent of H_2 by evaluating the constant inclination of the rear part of the temperature curve, and H_2 determines the absolute temperature rise of the probe. It can also be found by fitting the measured temperature profile obtained from an active heater experiment using a finite difference model.

The thermal conductivity of the "gap" between borestem and external medium is related to the thermal conductance H_2 by the relation (Langseth et al., 1972a)

$$\lambda_c = H_2\left(b+\frac{\Delta r}{2}\right)\ln\left(\frac{b+\Delta r}{b}\right) \tag{50}$$

The actual thickness Δr of the gap was reported to be in the millimeter size range and consisted of loose material with a thermal conductivity about six times smaller than that determined for the undisturbed lunar regolith. Therefore, it indeed acted as a thermal resistance for the flow of heat into the undisturbed regolith.

In this context, one should note that Langseth et al. (1976) later doubted the accuracy of the active thermal conductivity measurements as outlined above and, instead, based their estimates of lunar heat flow on a thermal conductivity value deduced from the propagation of the solar heat wave through the regolith.

4.4. TECP thermal probe on the Phoenix mission

After the completion of the Apollo missions in the 1970s no further *in situ* extraterrestrial measurements associated with heat flux and thermal properties could be made for more than 30 years, due to a lack of appropriate lander missions. Only in 2008 the NASA *Phoenix* mission, which delivered a lander in the north polar area of Mars offered the first opportunity to measure thermal properties on another extraterrestrial body. The TECP (*thermal and electrical conductivity probe*) was mounted on a moveable robotic arm, which allowed the instrument to reach several positions in the near vicinity of the lander (Zent et al., 2009, 2010). Fig. 12 shows the appearance and the dimensions of the instrument.

TECP is a remarkably multi-purpose device: It consists of four only 15 mm long steel needles positioned in a line along the downward pointing side of the electronics box with a mutual distance of about 7 mm. The thickness of the needles at the upper end is 3 mm. For a measurement, the needles are pushed into the ground in order to have reasonably good contact with the surrounding surface soil. Aside of thermal properties, the

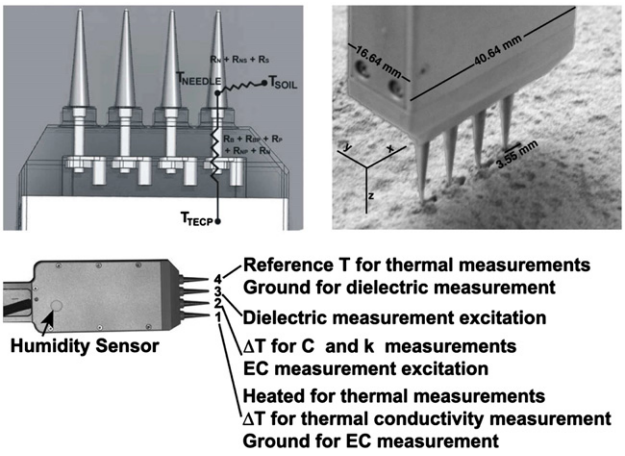

Fig. 12. The Phoenix TECP instrument consisting of the four needles pushed into the soil for a measurement and the adjacent electronics box (after Zent et al., 2009).

instrument can also retrieve information on electrical conductivity, dielectric permittivity and humidity of the surrounding soil.

Inspecting Fig. 12 one can immediately see that the geometry of the instrument differs strongly from a classical line heat source. The needles are "short and thick" and rather of a conical than of a cylindrical shape. For a thermal properties measurement one of the outermost needles (1 in Fig. 12) is heated actively and the temperature response both of the heated needle and two of the adjacent needles (the immediate neighbor and the most distant one) is recorded over a time period including the heating and the cooling phase.

Due to the complicated geometry, evaluation of thermal properties of the soil cannot be done in a straightforward way, as it would be possible with a standard needle probe. Rather, special calibration measurements are necessary, that relate the true properties of the soil to the ones evaluated from measurements by a model based on the "heated needle" theory. As described in detail by Zent et al. (2009) and Cobos et al. (2006), the relevant calibration coefficients can be obtained by measuring the temperature variation of the needles as a function of time both during the heating phase and during the subsequent cooling phase (after turn-off of the heat source). Note that the temperature recorded by the most distant needle (opposite of the heated one) is always taken as reference temperature. Using the expressions from the basic line heat source theory one can calculate the temperature increase $\Delta T(t)$ as

$$\Delta T(t) = -\frac{Q}{4\pi\lambda} Ei\left(\frac{-r^2 C_V}{4\lambda t}\right) \tag{51}$$

for the heating branch and

$$\Delta T(t) = -\frac{Q}{4\pi\lambda}\left[-Ei\left(\frac{-r^2 C_V}{4\lambda t}\right) + Ei\left(\frac{-r^2 C_V}{4\lambda (t-t_1)}\right)\right] \tag{52}$$

for the cooling branch.

There are two free parameters in these functions: thermal conductivity λ and volumetric heat capacity C_V. These two parameters must be varied systematically by an iterative procedure to find the minimal deviation from the known values of the calibration material. The advantage of this instrument is that one can use both the temperature record from the heated needle and that from the neighboring (not heated) needle. This increases the confidence of the derived "best fit" values for λ and C_V. To obtain a calibration curve over the whole range of λ and C_V range to be expected one needs to select different well-known calibration materials. In the case of TECP five different materials were used for calibration, from a glass ceramic with $\lambda = 1.4$ W m^1 K^{-1} on the high conductivity side to a highly insulating material with $\lambda = 0.03$ W m^1 K^{-1} (expanded polystyrene) on the low conductivity side. At the end of the fitting procedure with the calibration materials one obtains correlation formulae relating the true values of λ and C_V with the values obtained from the fitting procedure described above. As can be seen from the figures presented in Zent et al. (2009), there is a remarkably good linear fit between the known thermal parameters of the calibration materials and the values derived from measurements with the TECP instrument. This demonstrates the reliability of the applied procedure and at least gives some confidence for the construction of similar devices in the future.

4.5. MUPUS probe on the Rosetta/Philae mission

ESA's cornerstone mission *Rosetta*, which carries the lander *Philae* as a piggy-back payload, will hopefully be the next mission from which we can expect new data on the thermal properties of an extraterrestrial body. *Rosetta* was launched on March 02 2004 and is expected to arrive at its target comet P/Churyumov-Gerasimenko in August 2014. It is planned to deliver the lander *Philae* to the surface of the comet nucleus on November 20 2014 (Glassmeier et al., 2007). It carries a total of 10 instruments, among them MUPUS (*multi-purpose sensor for surface and subsurface science*). Its main task is to characterize the thermo-physical properties of the comet nucleus surface and possibly to detect layers of different composition and cohesive strength (Spohn et al., 2007). Note that comets are assumed to be porous mixtures of ice and minerals with a probably very low thermal conductivity. Laboratory measurements with porous ice samples gave values in the range $\lambda = 0.01-0.1$ W m^{-1} K^{-1} (Seiferlin et al., 1996). Recent remote sensing measurements at comet P/Tempel 1 revealed an upper limit for the surface thermal inertia ($I = \sqrt{C_V \lambda}$) of $I < 50$ J m^{-2} K^{-1} s$^{-1/2}$ (Groussin et al., 2007). This value corresponds to $\lambda < 0.005$ W m^{-1} K^{-1}.

The different components of the MUPUS instrument are summarized in Fig. 13. The main part is a penetrator consisting of a sharply tipped rod of about 32 cm length, which will be deployed in the cometary soil in vertical direction by a recoilless hammering device, after it has been positioned by a special deployment mechanism to a place about 1 m sideways of the lander (Grygorczuk et al., 2009a). In addition MUPUS includes an

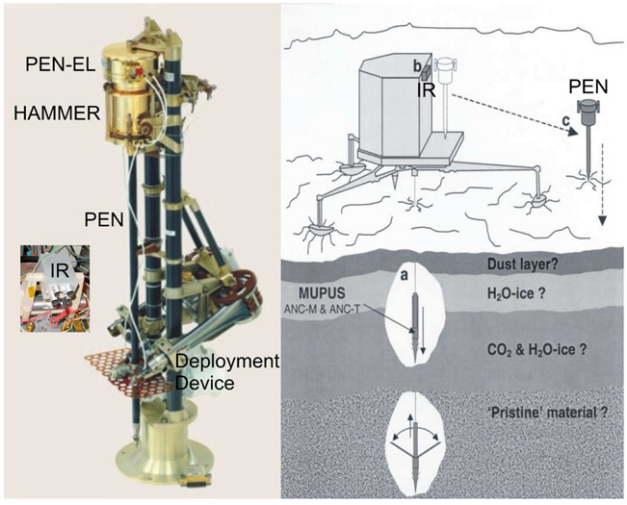

Fig. 13. The ground reference model of the thermal properties probe MUPUS (left). The original (flight model) is part of the payload of the Rosetta lander Philae, which is presently on its way to comet Churyumov-Gerasimenko, where it is expected to arrive in 2014. A schematics of the components as they are mounted on the lander is shown on the right side (after Spohn et al., 2007).

IR-sensor for measuring the surface temperature (mounted on the main body of the lander) as well as an accelerometer and an additional temperature sensor integrated into both of the two anchors (Thiel et al., 1999).

The two main measurement objectives of the penetrator after its deployment into the cometary soil are: (i) to measure the temperature versus depth profile and (ii) to measure the vertical thermal conductivity and diffusivity profile at the landing site, both as a function of time and of heliocentric distance. A major driver of the penetrator design was the minimization of the thermal disturbance introduced into the medium by the penetrator itself, which acts as a thermal shortcut or heat pipe. Therefore, the penetrator body is made of a hollow glass fiber composite tube of low thermal conductivity, with an outer diameter of 10 mm and a wall strength of 1 mm. It is equipped with 16 individual sensor/heater elements. These are mounted to the inner wall of the rod for protection of the sensors during the insertion process. The cylindrically shaped sensor elements consist of 0.5 μm thick titanium layers sputtered onto a 50 μm thick Kapton foil. They work as resistance temperature detectors with a nominal resistance of 100 Ohm at 0 °C and a temperature coefficient of resistance (TCR) of 0.002 K^{-1}. They can be used simultaneously for temperature sensing and heating. The TCR of these sensors is only about 1/2 compared to the tabulated value for bulk titanium, because surface effects become important for the thin layers used. The electrical connections of the sensors are realized as thin copper tracks which are printed onto the same Kapton foil. To minimize the total copper cross section, and thus the heat pipe effect of the penetrator, the sensor resistances are read out in a 2-wire configuration with a common return track. For electrical insulation the sensor foil is covered by additional Kapton on both sides and fixed to the interior of the tube wall. The length of the individual sensors is variable, from 10 mm close to the upper end (comet nucleus surface) to about 40 mm near the tip. This configuration has been chosen in order to achieve a better depth resolution of the thermal profile near the surface, where the temperature gradient is expected to be much steeper than at greater depth.

According to the measurement objectives the instrument can be operated in two modes: (i) a passive mode, where only the "natural" temperature variation in the vicinity of a particular sensor is measured in much the same way as standard platinum resistance thermometers are operated. In this way one obtains a temperature profile as a function of depth and time and can follow the natural temperature variations of the near surface layer over time (e.g. diurnal or seasonal heat waves). (ii) To perform "active" thermal conductivity measurements analogous to those done with the needle probes described in the previous sections.

Each of the sensors can also be supplied with a stronger power over a defined time span, so that it acts as a source of heat in the medium. The supplied power can be adjusted to the needs quasi-continuously between 0 and 1.5 W and, furthermore, a freely configurable number of sensors can be heated quasi-simultaneously. The idea behind such a configuration of heater and sensing elements is that it should be possible to acquire information on the vertical variation of thermal properties over a depth range which corresponds to the overall length of the penetrator, by heating individual sections sequentially.

There exist several factors affecting the achievable precision and the interpretation of the measurements. Concerning the temperature measurements, one important factor is the already mentioned heat pipe effect of the penetrator. Due to its probably larger thermal diffusivity compared to the medium the temperature gradients existing in the undisturbed medium are smoothed out. This is a general problem for all accurate soil temperature measurements, but especially important in this case because of the expected low conductivity of comets and the possibly rather poor thermal coupling to the surrounding granular material. A correction method for this effect has been suggested by Hagermann and Spohn (1999), who employed a solution of the inverse heat conduction problem.

Another MUPUS-specific problem is that the penetrator's front end electronics (PEN-EL) controlling all measurements and located on top of the golden cylindrical housing of the hammering device (see Fig. 13) requires a minimum operating temperature of −55 °C. This is considerably higher than the expected temperature of the cometary surface during nighttime. Although the heat conduction between PEN-EL and the penetrator rod has been reduced by the thermal design of the instrument, a certain non-negligible amount of heat still enters the penetrator tube from the top and influences the temperature readings of the upper sensors. An accurate numerical model of the whole penetrator system is needed to compensate for this error. Furthermore, the 2-wire method of resistance measurement has the drawback that an additional correction for the wire resistance is needed. Because the resistance of the copper tracks is also temperature-dependent, an iterative solution is required.

One difficulty of the MUPUS thermal properties measurements is also that the individual heater elements are rather short hollow cylinders than long and thin tubes embedded in the medium. Therefore, one is again faced with the problem that the standard hot needle theory cannot be applied in a straightforward way. Here, the capability of MUPUS to heat several neighboring sensors simultaneously with individually adjusted power settings enables the application of a "guarded torus" method (Seiferlin, 2006) where the outer "guard" heaters focus the flow of heat emanating from the central heater into an approximately radial flow. In this way the complexity of the problem is reduced locally to 1D and either analytical formulae for infinitely long cylindrical heat sources with finite diameter or simplified numerical models could be used for the interpretation.

Furthermore, two other factors complicate the interpretation of the penetrator measurements as the desired undisturbed values of the comet's thermal conductivity: (i) the penetration process leads to displacement of material and subsequent compaction of the surroundings, (ii) the applied heating could lead to sublimation of ice in the vicinity of the penetrator, especially if highly volatile phases like CO_2 or CO are also present in the ice/dust mixture. To overcome these problems the heating times should be maximized and the amount of heat introduced into the medium should be reduced as much as possible. However, in practice these approaches are limited on the one hand by the available energy on the lander and on the other hand by the noise of the temperature measurements (about 15 mK for MUPUS). The calibration of the MUPUS PEN and the results from laboratory and field tests of the instrument carried out in terrestrial snow and soil are described in Marczewski et al. (2004). Some information concerning this point can also be found in the overview paper by Spohn et al. (2007).

During the measurement phase of the *Philae* lander on the comet, not only the penetrator but also the anchors will be used by MUPUS to determine the thermal properties of the cometary material. When the anchor has come to rest at a certain depth, the temperature of the anchor will equilibrate to the ambient temperature. Recording the temperature decay by the Pt100 temperature sensor mounted inside the anchor then provides a means of determining the thermal diffusivity at the final anchor depth (Paton et al., 2010). This measurement will probably provide information on cometary thermal properties from a greater depth than the penetrator. In case of low thermal conductivity, the anticipated penetration depth of 1 m or more

might even be larger than the skin depth of the orbital heat wave, which implies that thermally unaltered pristine cometary material could be sampled.

In addition to the MUPUS thermal probe a similar instrument called EXTASE has been designed and built in the frame of a separate project (Schröer, 2006). The EXTASE probes comprise the same configuration of thermal sensors as the MUPUS experiment, but do not include a hammering and deployment device, since they were developed for terrestrial and laboratory applications. Thus lab and field measurements with the EXTASE probes offer a very useful opportunity to test the performance and evaluation of thermal conductivity measurements with MUPUS type probes, without having to deal with the full complexity of a space application.

4.6. Thermal sensors on Lunar-A

In addition to the instruments described in the previous sections, a few studies for devices designed to measure thermal properties of planetary surface layers have been undertaken in the recent past. One of these instruments was developed and tested to a mature stage and was planned to be flown on the Japanese Moon penetrator mission *Lunar-A* (Mizutani, 1995; Mizutani et al., 1995), which was unfortunately canceled. However, an instrument based on the heritage of the *Lunar-A* development might be flown in a similar configuration in the future. The goal of the *Lunar-A* thermal experiment was a reliable determination of the lunar heat flux by determining the subsurface temperature gradient and the thermal conductivity of the regolith. However, being an unmanned robotic mission, the setup is quite different from that of the Apollo heat flow experiment (Tanaka et al., 1999). Temperature sensors and heaters are mounted along the outer shell of a penetrator, which has been designed to impact the lunar surface vertically at a velocity of approximately $300\ \mathrm{m\ s^{-1}}$, thereby burying itself in the lunar regolith to a depth of at least one meter. A sketch of the penetrator indicating the positions of temperature and thermal conductivity sensors is shown in the lower part of Fig. 14.

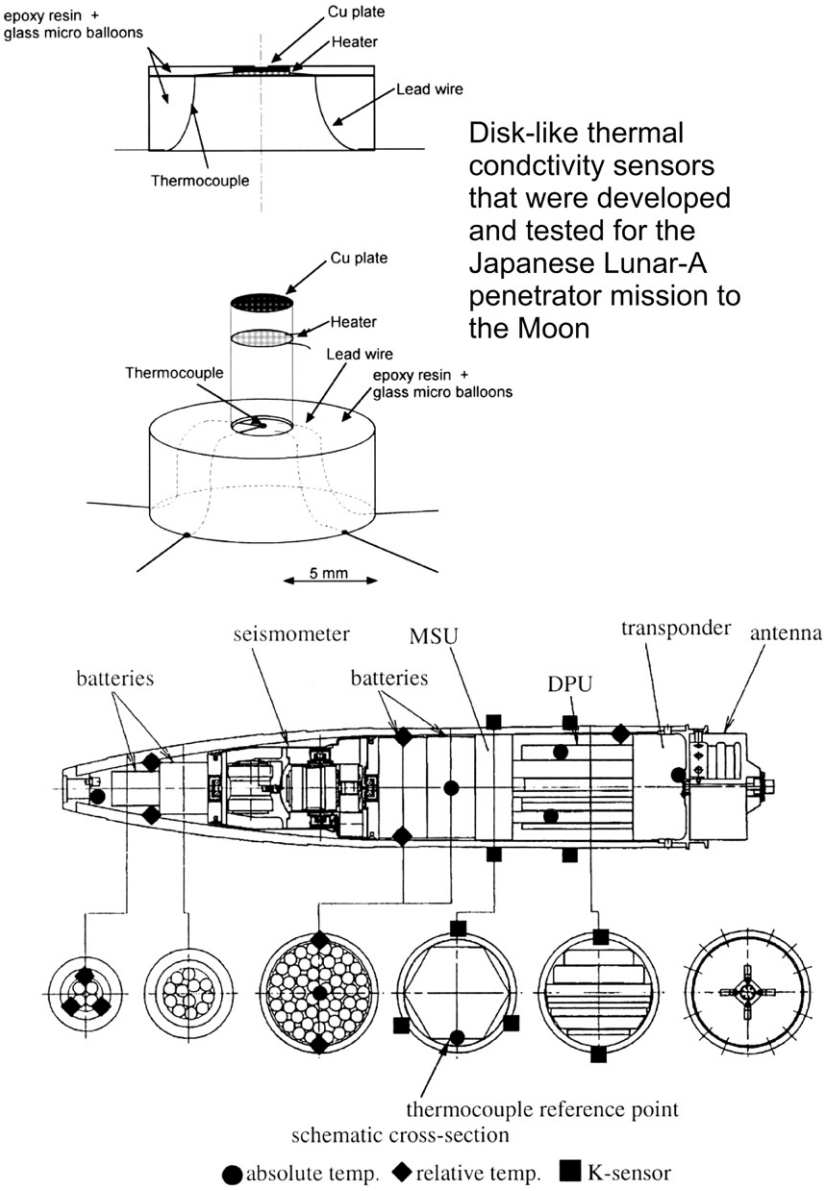

Fig. 14. Flat (disk-like) thermal conductivity sensors mounted on the Lunar-A penetrator developed by the Japanese space agency for the planned use on a lunar penetrator mission (top: after Hagermann et al., 2009; bottom: after Hagermann, 2005).

The penetrator has an overall length of approximately 80 cm and a circular cross section with a diameter of 14 cm.

The thermal property sensors mounted on the shell of the penetrator (shown in Fig. 14, upper part) consist of a copper plate embedded in a composite material of glass micro-balloons and epoxy resin. The lower face of the copper plate is in contact with a heater, and the entire sensor is glued to the penetrator body. The outer surface of the copper plate would be in contact with the regolith once the penetrator is successfully emplaced in the lunar soil.

This system was designed to be mechanically robust (otherwise it would not survive the impact), but again its geometry is far from a line heat source or a slender hollow cylinder. To evaluate thermal properties, in particular the thermal conductivity of the regolith, two types of studies have been undertaken, which might be useful for future applications. First, Horai et al. (1991) developed an analytical method for finding the thermal inertia of the surrounding material, using the initial slope of the temperature versus time curve. Their solution is based on formulae given in Carslaw and Jaeger (1959) for a disk heater clamped between two half spaces. Hagermann et al. (2009) however pointed out that this method must be considered with great care, because especially in the initial part of the heating curve the temperature response is very sensitive to (unpredictable) inhomogeneities in the space surrounding the sensor. Therefore, they developed and described an alternative, potentially more robust procedure, which has some similarity with the method used for the evaluation of the *Phoenix* TECP experiment. For each measured temperature curve, the residual between measured temperature in a particular time interval and the temperature calculated by a numerical model (where the parameters λ and C_V are varied over the range of interest) is calculated and plotted. Then one tries to minimize this function over the (λ, C_V) parameter space, using the measured temperature values both from the rising part (period where the sensor is actively heated) and from the declining part (period where the sensor cools down again). It turns out that this method is very sensitive with respect to λ, but has a low sensitivity w.r.t. C_V. Therefore, λ can be determined quite well, even when C_V is not accurately known.

Of course, to obtain quantitatively correct values, one has to perform calibration measurements with well known materials, spanning the range of interest for λ. The calibration materials used in this case were styrofoam ($\lambda = 0.036$ W m^{-1} K^{-1}), rubber ($\lambda = 0.244$ W m^{-1} K^{-1}) and glass ($\lambda = 1.398$ W m^{-1} K^{-1}). The advantage of the *Lunar-A* thermal sensors as compared to other designs is that no mechanical action other than the penetrator impact itself is necessary to obtain thermal and heat flux measurements. As in the case of Bullard's probe and the Apollo heat flux measurements some heat will be generated by the impact of the penetrator and one will have to extrapolate to the undisturbed status when trying to derive the natural temperature gradient. However, this temperature decay curve can be recorded and fitted by the formulae for a cylindrical tube given earlier in the paper. Thus, with a sufficiently accurate penetrator thermal model, the cooling curve can be used to derive some sort of bulk estimate for the regolith thermal properties.

4.7. Thermal sensors on HP^3-Mole

Another instrument which is currently under development (for use on Mars and/or the Moon) is the so-called *heat flow and physical properties package* (HP^3), which was originally proposed as part of the payload for a Mercury lander to be flown with ESA's Mercury mission *BepiColombo* (Spohn et al., 2001). After the lander segment was canceled, efforts to develop a similar instrument for application on Moon and Mars have been continued and HP^3 became part of the *Humboldt* payload onboard ESA's *ExoMars* mission, until the entire geophysical package was descoped in early 2009. In the course of the *ExoMars* development, HP^3 has successfully completed a phase B study and the current design has reached a quite mature technological level.

The deployed instrument is sketched in the left panel of Fig. 15 and the instrument is foreseen to dig into the near surface layers using an electro-mechanical *Mole* as a tractor. The principle of locomotion relies on the hammering energy to overcome the bearing capacity of the regolith at the mole-tip, while recoil forces are taken up by internal springs and, ultimately, wall friction. Therefore, locomotion does not directly depend on gravity and the *Mole* can be designed to operate successfully also in low gravity environments. Note, however, that the regolith's bearing capacity scales with lithostatic pressure and therefore penetration depth is also a function of the local gravitational acceleration.

The *Mole* concept was adopted and flight-proved for the PLUTO soil sampling device onboard ESA's *Beagle-2* lander (Richter et al., 2002), and has been further developed to include a payload compartment trailed behind the tractor mole. By interrupting the hammering cycles at given intervals, the instrument will thus be able to perform depth resolved measurements of the quantities of interest. In the current design, the HP^3 payload compartment carries a permittivity probe to determine the electrical properties of the regolith as well as heaters to measure the thermal conductivity of the regolith. However, a densitometer or other instrumentation could also be included. The instrument further includes an *instrumented tether*, which is equipped with temperature sensors to measure the thermal gradient in the soil, an *engineering tether*, which connects the instrument to the spacecraft, and the mechanical support structure providing secure storage of mole, payload compartment and tether during flight. Temperature sensors on the instrumented tether are designed to have a large surface area in order to increase thermal coupling to the surrounding regolith and two alternative designs have been investigated. Due to their small thickness, foil sensors are mechanically favorable, but these sensors are susceptible to bending stresses. Wired and thin film sensors are intrinsically more stable, but their

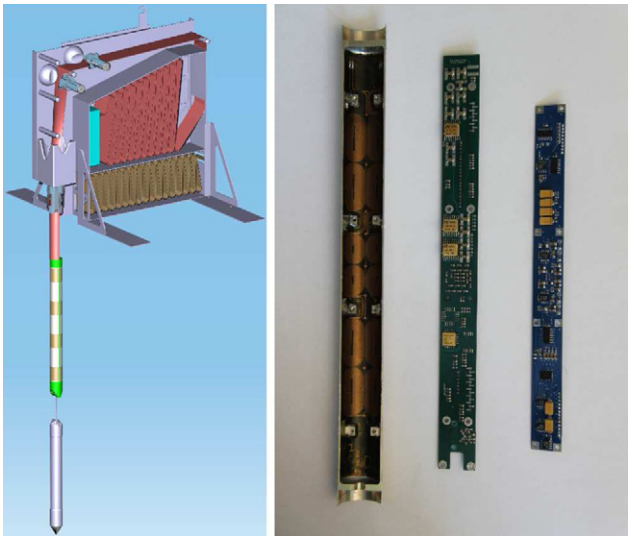

Fig. 15. Left: Sketch of the deployed HP^3 instrument showing the so-called tractor Mole (gray), the Payload Compartment (green), the Instrumented Tether (red), the Engineering Tether (brown), as well as the mechanical support structure. Right: One Payload Compartment half shell and Payload Compartment electronics boards. The Payload Compartment has a diameter of 26 mm and a length of 302 mm.

small size makes thermal coupling non-ideal. However, they can be mounted on copper patches to increase thermal coupling and this is the baseline design currently employed. Details of the payload compartment are given in the right panel of Fig. 15, which shows a payload compartment half shell including a heating foil glued to its inside. Furthermore, electronics boards for the mole's power supply and command handling (middle) as well as the *permittivity probe* electronics board (right) are shown.

Heating foils are glued inside the payload compartment and consist of copper circuits sandwiched between two layers of Kapton. The instrument will measure thermal conductivity using the cylindrically shaped compartment as a modified line heat source. As copper has a relatively large temperature coefficient close to $0.004\,K^{-1}$, heaters also serve as resistance temperature detectors and are used to simultaneously measure the compartment's temperature while heating. To compensate for heat loss in the axial direction, the temperature rise at the compartment is only measured at the central section, while the compartment is heated over its entire length.

Due to the deviation from the ideal line heat source geometry and the complex interior structure of the payload compartment, the standard evaluation method to determine thermal conductivity from the probe's self-heating curve (as illustrated in Fig. 5) cannot be directly applied. Rather, a physical model of the probe-regolith system taking the relevant heat paths and heat capacities into account must be used to invert the self-heating curves for the regolith's thermal conductivity (see e.g. Jones, 1988). An approach similar to that followed by Langseth et al. (1972b) will be adopted, who fitted the functional dependence of the self-heating curve using a numerical model. This approach has been shown to be robust with respect to the probe's thermo-physical properties, as well as the unknown contact resistance between the instrument and the surrounding regolith (Grott et al., 2010).

While having a smaller depth resolution than the MUPUS penetrator, HP^3 is able to measure thermal conductivity over a much larger distance to depths of up to 3–5 m. Together with a measurement of the thermal gradient using temperature sensors on the *instrumented tether*, HP^3 will be able to determine the surface heat flux of the Moon and Mars. Furthermore, since its locomotion does not rely on gravity, it could as well be used on minor bodies like asteroids and comets.

Another mole design with somewhat different features than those of the HP^3 mole has recently been developed and tested at the Space Research Centre of the Polish Academy of Sciences, Warsaw (Grygorczuk et al., 2009b).

4.8. Thermal sensors on Cassini/Huygens

The sensors outlined so far have been designed with measurements of solid materials in mind. A sensor designed for a different purpose was successfully flown during the *Cassini/Huygens* mission. The THP (thermal properties) experiment was part of the Surface Science Package of the *Huygens* probe (Zarnecki et al., 2005). Its sensors were designed to measure the thermal conductivity of the tentative oceans on Titan's surface as well as the atmosphere. THP consisted of two pairs of 5 cm long platinum wires which were enclosed in cylindrical cells to minimize the effect of gas/liquid flow. The pairs were slightly different in dimensions, one being designed for thermal measurements in air, the other for measurements in a liquid. Thus, the wire and cell radii were slightly different. The wire radius was 5 μm for the gas cells and 12.5 μm for the liquid cells. The operating principle was again the hot wire method (see e.g. Healy et al., 1976). This means a wire was heated using a constant current and the wires' change in resistance was then measured as an indication of temperature and thus thermal conductivity of the surrounding medium (Hathi et al., 2007). The sensor worked nominally during the descent of the *Huygens* probe towards Titan's surface and made measurements from approximately 30 km altitude downwards. Thermal measurements pointed towards some liquid deposition within the sensor capsules, which was attributed to either condensation or passing through layers of fog or clouds (Hathi et al., 2008).

5. Discussion and conclusions

In the preceding sections we have reviewed various designs for thermal sensors, which have been constructed and used for measuring either the thermal properties of materials and/or the heat flux from the interior of planetary bodies, which is of primary interest for understanding solar system evolution. While the hot needle method is standard for determining the thermal conductivity of homogeneous (porous or non-porous) materials in a controlled laboratory environment and sometimes in the field, it cannot be employed in an easy way on a planetary surface. Only a few designs have been used on planetary missions up to now, among them the Apollo *heat flow and thermal conductivity experiment* HFE (on *Apollo 15* and *Apollo 17*) and the recent *Phoenix* physical properties probe TECP. While the former was inserted into a pre-drilled borehole and used to determine both thermal conductivity and lunar heat flux, the latter was able to measure thermal conductivity and heat capacity of the Martian soil in the uppermost 2–3 cm. The geometry of both designs was quite different from that of a thin needle sensor, therefore an elaborative evaluation procedure was necessary to derive the parameters of interest. The third design that has been developed for space applications is the so-called MUPUS penetrator mounted aboard the lander *Philae* of ESA's cornerstone mission *Rosetta*, which is currently on the way to its target comet. Again, this is not a standard hot needle sensor, but rather a sequence of short hollow cylinders, that can be heated independently. This construction will allow to obtain some information on the variation of thermal properties with depth. But again, interpretation of the data will not be easy and demands to apply detailed numerical modeling rather than a standard evaluation procedure.

As we can conclude from the descriptions given above there exist a couple of methods to determine the thermal properties (in particular thermal conductivity) of materials as well as the heat flux from a planetary interior by *in situ* methods. All of them are based on accurate temperature measurements at well defined positions.

Concerning the evaluation of heat conductivity, the most frequently used method is the so-called line heat source method, where a long and thin needle is inserted into a homogeneous medium and heated with a constant power. The advantage of this method is the easy way to determine thermal conductivity from a simple temperature measurement: on a semi-logarithmic plot (needle temperature versus $\ln t$), after an initial nonlinear part the temperature increase should become linear and the inclination of the curve is inversely proportional to the thermal conductivity of the surrounding medium.

The formulae used for the thin needle method are derived from a more general theory of heat conduction in axisymmetric cylindrical systems, for which analytic solutions are known. These are cylinders with a finite radius, which can be heated either instantaneously by a heat source or by a constant power source over a finite time.

Geophysical probes with the aim to measure the heat flux from the Earth's interior *in situ* have been constructed and used first in the 1950s in the pioneering work of Bullard (1954). He used a several meters long steel tube with a diameter of 27 mm, which was equipped with two thermocouple junctions. This heavy rod was rammed into the ground of the Atlantic Ocean

and used to measure the vertical temperature gradient across the uppermost meters below the sea floor with high accuracy. These measurements allowed him to derive the intrinsic heat flux from the Earth interior largely unaffected by diurnal and seasonal variations.

While heat flux measurements from the Earth's interior and their variations are in the meantime well monitored, the situation is very different for extraterrestrial planetary bodies. Here there exist to date very limited data. Actually, *in situ* measurements of the interior heat flux and the thermal conductivity of the near surface layer have only been performed for the Moon in the frame of two Apollo missions (*Apollo 15* and *Apollo 17*) in the years 1971 and 1972. They carried a surface science package named ALSEP, which included a thermal conductivity and heat flow probe inserted into a pre-drilled borehole. Another data set was added recently by the TECP-instrument of NASA's successful Mars mission *Phoenix*, which delivered a lander in the vicinity of the north polar cap of Mars.

Instruments with the aim to measure the interior heat flux and the thermal conductivity of planetary bodies have also been designed and built for other space missions. These include designs that deviate significantly from the heated needle method. The experiment MUPUS is a sensor aboard the comet lander *Philae*, which currently flies aboard ESA's comet mission *Rosetta*. This sensor will be hammered into the surface of the comet nucleus to a depth of 32 cm. Over this depth it can measure the natural temperature variations with a resolution of a few centimeters. As the individual temperature sensors can also act as heaters in this instrument, it may also be able to retrieve at least some crude information on the thermal conductivity of individual near surface layers (for example discern a dust mantle with very low conductivity from a cohesive layer still containing sintered ice). Other concepts of thermal sensors that have been developed for future missions are heated disks with a flat geometry. Such a system was developed and tested for the Japanese penetrator *Lunar-A*. Although the *Lunar-A* mission could not be completed as originally planned, these developments might be used for other lunar or planetary missions.

In summary, one can say that there are two basically different evaluation methods to derive thermal properties from measured temperature profiles in heated probes: (i) Semi-analytic models based on the properties of axisymmetric configurations and (ii) fully numerical models using e.g. finite element or finite difference approximations of the heat conduction equations and boundary conditions.

5.1. Cylinder-symmetric solutions

Since most of the "active" probes built for field measurements and/or space applications have a cylinder-symmetric geometry, the evaluation methods make use of the cylinder-symmetric solutions of the heat conduction equation. The most popular method for measuring and evaluating the thermal conductivity of a material is the *hot needle* method, where thermal conductivity can be calculated by a simple algebraic formula from the measured temperature rise of the sensor in response to a known heat input. However, this formula can only be applied unambiguously if:

- The material where the sensor is imbedded has a homogeneous structure over the length of the heated part and does not undergo phase transitions (like melting, sublimation, etc.) during the time of the measurement. In particular this means that any layering would disturb the measurement.
- The natural temperature gradient in the material over the length of the sensor is negligible.
- The length/diameter ratio of the sensor is reasonably high (about 20:1 minimum), so that the sensor can be approximated as an infinitely long thin wire and axial losses are negligible.

From the discussion in the previous sections it appears obvious that it cannot be taken for granted that all these conditions are safely fulfilled, especially when such measurements are performed on the unknown surface of a planetary body or a comet nucleus. While the assumption of a cylinder symmetric configuration is fulfilled in most of the sensors constructed for extraterrestrial applications, the geometry of the heaters used in the Apollo thermal probes as well as the heater elements comprising the *Rosetta/Philae* MUPUS probe is strongly deviating from a slender needle geometry and therefore axial heat losses play a much bigger role. This should be expected even to a much higher extent, since the thermal conductivities derived for the lunar regolith from the Apollo *heat flow and thermal conductivity experiment* are extremely low, due to the high vacuum environment. Nevertheless, as noted by Langseth et al. (1972a,b), the heating curves obtained from the Apollo thermal conductivity measurements in the lunar regolith could be fitted quite well by an algebraic relation very similar to the one used for the heated needle probe, for heating times exceeding 20 hours. This lends some credibility to the view that—with appropriate calibrations and comparison measurements—the standard line heat source theory can be applied to some extent also in the case of short (cylindrically shaped) heaters, if reasonably long heating times are applied. The same conclusion was found by Kömle et al. (2010) based on laboratory measurements with a hollow cylindrical sensor. Nevertheless—when reviewing the existing literature both of the "space community" and in other fields where thermal conductivity measurements are important (e.g. soil and rock physics, food production and storage, geo-engineering, etc.) the influence of axial heat losses on the accuracy of thermal conductivity measurements has to date received little attention. Both in the papers associated with the Apollo measurements and in the work done up to now for a proper interpretation of the MUPUS measurements either the integral solutions given by Carslaw and Jaeger (1959) or the standard line heat source formula have been applied, ignoring largely the influence of axial losses. Interestingly, from the classical papers of the 1950s only in the work by Blackwell (1953, 1954) the problem of axial heat losses in a thermal conductivity measurement is treated in some detail, but for a different geometry (rectangular slab rather than axisymmetry). However, as noted by the author himself, *the problem of the axial flow error, etc.* was *not completely solved*. In a recent paper Seiferlin (2006) has addressed this question again and proposed a way to compensate for it by using the so-called guard heaters in addition to the main heating element, from which the thermal conductivity is derived.

5.2. Fully numerical models

With the rapid development of computer-aided computational tools a vast field of new possibilities opened up for a more detailed evaluation of thermal measurements. First, while it still remains extremely useful to build new models based on the classical axisymmetric formulae given in the papers by Jaeger and the other pioneers, it is now much less time-consuming to calculate solutions including the numerical evaluation of integrals involving Bessel functions. While Bullard and others had to evaluate these integrals in a cumbersome way and finally produced tables with a rather rough parameter resolution, with today's computing possibilities these tasks can be done much faster and more efficient. Moreover, we are not necessarily

restricted to axisymmetric configurations, but can produce numerical solutions in a quite arbitrary geometry.

Finite element software packages like e.g. COMSOL or ANSYS[4] are able to solve the heat conduction equation with the appropriate boundary conditions on a numerical grid of variable cell size and also allow to study non-axisymmetric configurations. Heat sources are not necessarily restricted to line or surface sources, but can also be modeled as volume sources with a finite extent. Nevertheless the semi-analytic solutions compiled in Carslaw and Jaeger (1959) and the other reference articles cited before remain important, because they describe benchmark cases that can be compared with corresponding numerical solutions, in order to judge the quality and accuracy of the numerics.

Acknowledgments

This work was supported by the Austrian *Fonds zur Förderung der wissenschaftlichen Forschung* under the Translational Research Project L317–N14.

Appendix A. Temperature decay of the Apollo heat flow probes

We investigate the temperature evolution in a cylinder of infinite length which is composed of an inner cylinder of radius a (sensor, Region 1) and a cylindrical sheath (borestem, Region 2) of outer radius b, placed in an infinite medium (Region 3). The configuration is illustrated in Fig. 16a. Regions 1 and 2 are described by their specific heat S_n per cylinder length. In order that this description is valid, it has to be assumed that the cylinder is made of ideal conductors. More precisely, the thermal conductivity of the materials in Regions 1 and 2 must be so high that the temperatures (T_1 and T_2, respectively) do not vary spatially within these regions. The thermal property of the boundary between the inner cylinder and its mantle is described by the surface conductance H_1 (heat transferred per area, time and temperature jump at the boundary). Similarly, H_2 denotes the surface conductance of the boundary between the sheath and the surrounding medium. We further use the abbreviations (43), where the conductivity λ and the diffusivity κ describe the external medium in Region 3.

Our aim is to determine the temperatures $T_1(t)$, $T_2(t)$ and $T(r,t)$ in Regions 1–3, with their respective initial values T_{10}, T_{20} and T_∞ at $t=0$ being prescribed (the denotation T_∞ indicating that this is the temperature approached everywhere as $t\to\infty$). A closed form solution of the governing equations in the three regions is possible via Laplace transformation. For Region 3 the heat conduction equation and the boundary relation at $r=b$ are needed, which read

$$\frac{\partial^2\tilde{T}}{\partial r^2}+\frac{1}{r}\frac{\partial\tilde{T}}{\partial r}-\frac{p}{\kappa}\tilde{T}=-\frac{T_\infty}{\kappa} \tag{53}$$

$$\left.\frac{\partial\tilde{T}}{\partial r}\right|_b=\frac{H_2}{\lambda}(\tilde{T}|_b-\tilde{T}_2) \tag{54}$$

$(\cdot)|_b$ denoting the value of $(\cdot)$ at $r=b$. Here and in the following the tilde over a function signifies its Laplace transform with regard to time, using p as the independent variable of the transform. Due to the axial symmetry of the configuration, the temperature $T(r,t)$ and its Laplace transform

$$\tilde{T}(r,p)=\int_0^\infty T(r,t)e^{-pt}\,dt \tag{55}$$

[4] Websites: www.comsol.com and www.ansys.com.

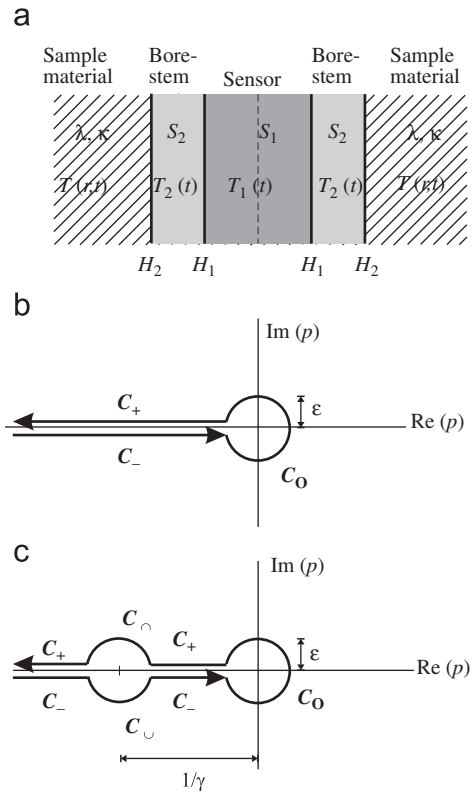

Fig. 16. (a) Sensor cylinder with bore-stem mantle in an infinite exterior medium. A finite cross-section containing the symmetry axis (dashed line) is exhibited, with bold lines indicating the boundaries of surface conductance H_1 and H_2, respectively. (b) Integration contour for inverse Laplace transform to obtain T and T_2. (c) Contour used for T_1, compassing the singularity $p=-1/\gamma$.

depend only on the radial distance r from the cylinder axis (and on t or p, respectively). The heat flow $q_1=2\pi aH_1(T_2-T_1)$ per cylinder length through the cylindrical boundary at $r=a$ determines the temperature change $\partial T_1/\partial t=q_1/S_1$ in Region 1. Similarly, the flows through the boundaries at $r=a$ and $r=b$ are responsible for the temperature change in Region 2. The Laplace transforms of the corresponding relations are

$$S_1(p\tilde{T}_1-T_{10})=2\pi aH_1(\tilde{T}_2-\tilde{T}_1) \tag{56}$$

$$S_2(p\tilde{T}_2-T_{20})=2\pi aH_1(\tilde{T}_1-\tilde{T}_2)+2\pi bH_2(\tilde{T}|_b-\tilde{T}_2) \tag{57}$$

where the Laplace transforms of the derivatives $\widetilde{\partial T_n/\partial t}=p\tilde{T}_n-T_{n0}$ are used. From these two equations $\tilde{T}_1$ and $\tilde{T}_2$ can be determined as functions of $\tilde{T}|_b$. The so obtained

$$\tilde{T}_2=\frac{\hat{y}+2\pi bH_2(1+\gamma p)\tilde{T}|_b}{\hat{z}} \tag{58}$$

is substituted into (54), yielding

$$\left.\frac{\partial\tilde{T}}{\partial r}\right|_b\frac{\hat{z}\lambda}{H_2}-\tilde{T}|_b\hat{x}+\hat{y}=0 \tag{59}$$

with $\hat{x}$, $\hat{y}$, and $\hat{z}$ being polynomials in the variable p,

$$\hat{x}=(S_1+S_2)p+S_2\gamma p^2 \tag{60}$$

$$\hat{y}=S_1T_{10}+S_2T_{20}+S_2T_{20}\gamma p \tag{61}$$

$$\hat{z}=2\pi bH_2+p(S_1+S_2+2\pi bH_2\gamma)+S_2\gamma p^2=\hat{x}+2\pi bH_2(1+\gamma p) \tag{62}$$

The solution of (53) is

$$\tilde{T}=\frac{T_\infty}{p}+g(p)\,K_0(qr) \tag{63}$$

with $q=\sqrt{p/\kappa}$ and K_0 being the modified Bessel function of second kind and zeroth order. For simplicity we put $T_\infty=0$ in the derivation, shifting all temperatures by T_∞ in the final result. This procedure is valid since the governing equations (53)–(57) are conserved under a shift of all temperatures appearing in them. $T(r,t)$ is obtained by applying the inverse Laplace transform to $\tilde{T}(r,p)$:

$$T=\frac{1}{2\pi i}\int_{\mathcal{C}} g(p)K_0(qr)e^{pt}\,dp \tag{64}$$

where the contour $\mathcal{C}$ is a straight line from $x-i\infty$ to $x+i\infty$ with $x>0$. Since the integrand is analytic with a branch cut along the negative real axis, the contour can be modified to the path shown in Fig. 16b. The path is divided into three parts, two straight lines parallel to the negative real axis ($\mathcal{C}_+$ above and $\mathcal{C}_-$ below the axis), and a circle $\mathcal{C}_\circ$ of radius ε around the origin. In the limit $\varepsilon\to 0$ the contribution of the integral along the circle vanishes, because $g(p)$ is finite at $p=0$, as will be shown in the following. Substituting (63) with $T_\infty=0$ into (59) we find $g(p)$ after reordering and taking $K_0'=-K_1$ into account,

$$g(p)=\frac{\hat{y}}{\hat{x}K_0(qb)+\frac{\lambda}{H_2}\hat{z}qK_1(qb)} \tag{65}$$

Let T_+ and T_- denote the contributions to T in (64) which stem from the contour parts $\mathcal{C}_+$ and $\mathcal{C}_-$, respectively. Although p runs through the same values on both paths, $q=\sqrt{p/\kappa}$ does not, as the square root has to be defined in such a way that from any point of $\mathcal{C}$ each other point on $\mathcal{C}$ must be reached by the same analytic continuation. The canonical definition is to let q be positive imaginary on $\mathcal{C}_+$ and negative imaginary on $\mathcal{C}_-$. This suggests the substitution $p=-\kappa x^2/b^2$, and $q_\pm=\pm ix/b$ with the upper/lower sign being used for $\mathcal{C}_\pm$. The integrals T_+ and T_- hence read

$$T_\pm=\pm\frac{1}{2\pi i}\int_0^\infty g_\pm(p)K_0(q_\pm r)\exp(-\tau x^2)\left(-\frac{2\kappa}{b^2}\right)x\,dx \tag{66}$$

where the subscript sign in $g_\pm(p)$ indicates whether q_+ or q_- is to be substituted for q in (65). By means of the Bessel functions relations

$$\begin{aligned} q_\pm^\nu K_\nu(q_\pm b)&=\left(\frac{xe^{\pm i\pi/2}}{b}\right)^\nu K_\nu(xe^{\pm i\pi/2})\\ &=-\left(\frac{x}{b}\right)^\nu\frac{i\pi}{2}e^{(\pm 1-1)\nu i\pi/2}H_\nu^{(2)}(xe^{(\pm 1-1)i\pi/2})\\ &=\left(\frac{x}{b}\right)^\nu\frac{i\pi}{2}e^{(\pm 1+1)\nu i\pi/2}H_\nu^{(1)}(xe^{(\pm 1+1)i\pi/2}) \end{aligned} \tag{67}$$

$H_\nu^{(1)}(z)=J_\nu(z)+Y_\nu(z)$ and $H_\nu^{(2)}(z)=J_\nu(z)-Y_\nu(z)$ we find

$$\begin{aligned} &[g_+(p)\;\;K_0(q_+r)-g_-(p)\;\;K_0(q_-r)]=\\ &\quad+\frac{\hat{y}H_0^{(2)}(xr/b)}{\hat{x}H_0^{(2)}(x)+\hat{z}hxH_1^{(2)}(x)}-\frac{\hat{y}H_0^{(1)}(xr/b)}{\hat{x}H_0^{(1)}(x)+\hat{z}hxH_1^{(1)}(x)}\\ &\quad=-2i\hat{y}\;\frac{Y_0(xr/b)[\hat{x}J_0(x)+\hat{z}hxJ_1(x)]-J_0(xr/b)[\hat{x}Y_0(x)+\hat{z}hxY_1(x)]}{[\hat{x}J_0(x)+\hat{z}hxJ_1(x)]^2+[\hat{x}Y_0(x)+\hat{z}hxY_1(x)]^2} \end{aligned} \tag{68}$$

Expressing $\hat{x}$, $\hat{y}$ and $\hat{z}$ in terms of the variable x and the symbols defined in (43),

$$\hat{x}=-\frac{\kappa}{b^2}(S_1+S_2)x^2[1-Ax^2] \tag{69}$$

$$\hat{y}=(S_1+S_2)\left[\frac{S_1T_{10}+S_2T_{20}}{S_1+S_2}-T_{20}Ax^2\right] \tag{70}$$

$$\hat{z}=-\frac{\kappa}{hb^2}(S_1+S_2)[-\alpha+(h+\alpha B)x^2-hAx^4] \tag{71}$$

we obtain an integral of a real function for the temperature evolution $T=T_+ + T_-$ in the external medium:

$$T=-\frac{2}{\pi}\int_0^\infty\frac{\hat{S}(x)[\hat{J}(x)Y_0(xr/b)-\hat{Y}(x)J_0(xr/b)]}{\hat{J}(x)^2+\hat{Y}(x)^2}e^{-\tau x^2}\,dx \tag{72}$$

with

$$\hat{S}(x)=\frac{S_1T_{10}+S_2T_{20}}{S_1+S_2}-T_{20}Ax^2 \tag{73}$$

$$\hat{J}(x)=x[1-Ax^2]J_0(x)+[-\alpha+(h+\alpha B)x^2-hAx^4]J_1(x) \tag{74}$$

$$\hat{Y}(x)=x[1-Ax^2]Y_0(x)+[-\alpha+(h+\alpha B)x^2-hAx^4]Y_1(x) \tag{75}$$

Taking the relations $J_0'(x)=-J_1(x)$, $Y_0'(x)=-Y_1(x)$ and $J_1(x)Y_0(x)-Y_1(x)J_0(x)=2/(\pi x)$ into account, the temperature and its gradient at the boundary $r=b$ approached from outside can be written as

$$T|_b=-\frac{4}{\pi^2}\int_0^\infty\frac{\hat{S}(x)[-\alpha+(h+\alpha B)x^2-hAx^4]}{x[\hat{J}(x)^2+\hat{Y}(x)^2]}e^{-\tau x^2}\,dx \tag{76}$$

$$\left.\frac{\partial T}{\partial r}\right|_b=-\frac{4}{\pi^2 b}\int_0^\infty\frac{\hat{S}(x)x[1-Ax^2]}{\hat{J}(x)^2+\hat{Y}(x)^2}e^{-\tau x^2}\,dx \tag{77}$$

Substitution of these boundary values in (54) yields the temperature T_2 in the cylindrical sheath (borestem),

$$T_2=\frac{4\alpha}{\pi^2}\int_0^\infty\frac{\hat{S}(x)[1-Bx^2]}{x[\hat{J}(x)^2+\hat{Y}(x)^2]}e^{-\tau x^2}\,dx \tag{78}$$

By means of (54) and (56) we determine $\tilde{T}_1$ as

$$\tilde{T}_1=\frac{\tilde{T}_2+\gamma T_{10}}{1+\gamma p}=\frac{\tilde{T}|_b-\frac{\lambda}{H_2}\left.\frac{\partial\tilde{T}}{\partial r}\right|_b+\gamma T_{10}}{1+\gamma p} \tag{79}$$

Applying the inverse Laplace transformation and utilizing $K_0'(z)=-K_1(z)$ leads to

$$T_1=\frac{1}{2\pi i}\int_{\mathcal{C}}\frac{g(p)\left[K_0(qb)+\frac{\lambda}{H_2}qK_1(qb)\right]}{1+\gamma p}e^{pt}\,dp+T_{10}e^{-t/\gamma} \tag{80}$$

where the last term is the inverse Laplace transform of $T_{10}\gamma/(1+\gamma p)$. In the above integral the integration contour C cannot be changed in the same way as in (64) due to the singularity of the integrand at $p=-1/\gamma$. Instead, one has to use the contour depicted in Fig. 16c, where additional semicircles $\mathcal{C}_\cap$ and $\mathcal{C}_\cup$ of radius ε compass $p=-1/\gamma$ above and below the real axis, respectively. The integral over the other parts of the contour can be treated in analogy to (64) as $\varepsilon\to 0$, i.e. the substitutions $p=-\kappa x^2/b^2$ and $q_\pm=\pm ix/b$ are applied to deal with the integrals over the straight lines $\mathcal{C}_+$ and $\mathcal{C}_-$ parallel to the negative real axis and the contribution of the circle $\mathcal{C}_\circ$ around the origin vanishes. According to (79) this procedure results in the integral (78) with its integrand divided by $1+\gamma p=1-Bx^2$. The integral over $\mathcal{C}_\cap$ can be calculated on the basis of the substitution $p=-1/\gamma+\varepsilon\exp(i\phi)$ with the angle ϕ running from 0 to π. In the limit $\varepsilon\to 0$ we have $\hat{x}\to -S_1/\gamma$, $\hat{y}\to S_1T_{10}$, $\hat{z}\to -S_1/\gamma$, and $g(p)[K_0(qb)+(\lambda/H_2)qK_1(qb)]\to-\gamma T_{10}$. Hence, the contribution of the contour $\mathcal{C}_\cap$ to T_1 converges to

$$\frac{1}{2\pi i}\int_0^\pi\frac{-\gamma T_{10}}{\gamma\exp(i\phi)}e^{-t/\gamma}\exp(i\phi)i\,d\phi=-\frac{T_{10}}{2}e^{-t/\gamma} \tag{81}$$

A similar derivation shows that the integral over $\mathcal{C}_\cup$ has the same limit. Hence, the contributions of $\mathcal{C}_\cap$, $\mathcal{C}_\cup$ and the term $T_{10}e^{-t/\gamma}$ in (80) cancel each other, leaving only the integrals over the straight lines parallel to the real axis. Thus, the final formula for the temperature in the sensor-region 1 becomes

$$T_1=\frac{4\alpha}{\pi^2}\int_0^\infty\frac{\hat{S}(x)}{x[\hat{J}(x)^2+\hat{Y}(x)^2]}e^{-\tau x^2}\,dx \tag{82}$$

In the special case where the sample and the borestem have the same initial temperature, $T_{10}=T_{20}=T_0$, one obtains $\hat{S}(x)=T_0(1-Ax^2)$, and

the result (82) coincides with (41) and (42) if the initially mentioned shift of temperatures by T_∞ is performed.

References

Abramovich, M., Stegun, I.A., 1972. Handbook of Mathematical Functions—With Formulas, Graphs and Mathematical Tables. Dover Publications, New York.

Banaszkiewicz, M., 2002a. Analytical model of a cylindrical thermal probe. Space Research Centre, Polish Academy of Sciences. Unpublished manuscript.

Banaszkiewicz M., 2002b. Analytical model of a multi-sensor thermal conductivity probe. Space Research Centre, Polish Academy of Sciences. Unpublished manuscript.

Banaszkiewicz M., 2002c. The multi-sensor thermal probe in a layered medium. Space Research Centre, Polish Academy of Sciences. Unpublished manuscript.

Banaszkiewicz, M., 2002d. Temperature profile determination from measurements of a penetrating thermal probe. Space Research Centre, Polish Academy of Sciences. Unpublished manuscript.

Banaszkiewicz, M., 2002e. Multi-sensor thermal probe in a non-axially symmetric geometry. Unpublished manuscript.

Banaszkiewicz, M., Seweryn, K., Wawrzaszek, R., 2007. A sensor to perform in-situ thermal conductivity determination of cometary and asteroid material. Advances in Space Research 40 (2), 226–237. doi:10.1016/j.asr.2007.05.037.

Blackwell, J.H., 1953. Radial–axial heat flow in regions bounded internally by circular cylinders. Canadian Journal of Physics 31, 472–479. doi:10.1139/p53-046.

Blackwell, J.H., 1954. A transient flow method for determination of thermal constants of insulating materials in bulk. Part I: theory. Journal of Applied Physics 25, 137–144. doi:10.1063/1.1721592.

Bayin, S.S., 2006. Mathematical Methods in Science and Engineering. Wiley (Chapters 18 and 19).

Bullard, E., 1954. The flow of heat through the floor of the Atlantic Ocean. Proceedings of the Royal Society of London. Series A, Mathematical and Physical Sciences 222 (1150), 408–429. doi:10.1111/j.1365-246X.1937.tb07120.x.

Carslaw, H.S., Jaeger, J.C., 1959. Conduction of Heat in Solids. Oxford University Press.

Cobos, D.R., Campbell, G.S., Campbell, C.S., 2006. Modified line heat source for measurement of thermal properties on Mars. In: Dinwiddie, R.D. (Ed.), Proceedings of the 28th International Thermal Conductivity Conference. Destech. Publ., Lancaster, PA, pp. 331–338.

Courant, R.D., Hilbert, R.D., 1962. Methods of Mathematical Physics, vol. 2. Interscience, New York.

Glassmeier, K.H., Boehnhardt, H., Koschny, D., Kührt, E., Richter, I., 2007. The ROSETTA mission: flying towards the origin of the solar system. Space Science Review 128, 1–21. doi:10.1007/s11214-006-9140-8.

Goodhew, S., Griffiths, R., 2004. Analysis of thermal-probe measurements using an iterative method to give sample conductivity and diffusivity data. Applied Energy 77, 205–223. doi:10.1016/S0306-2619(03)00122-3.

Grott, M., Knollenberg, J., Krause, C., 2010. The Apollo Lunar heat flow experiment revisited: a critical reassessment of the in-situ thermal conductivity determination. Journal of Geophysical Research 115, E11005. doi:10.1029/2010JE003612.

Groussin, O., A'Hearn, M.F., Li, J.Y., Thomas, P.C., Sunshine, J.M., Lisse, C.M., Meech, K.J., Farnham, T.L., Feaga, L.M., Delamere, W.A., 2007. Surface temperature of the nucleus of Comet 9P/Tempel 1. Icarus 191, 63–72. doi:10.1016/j.icarus.2006.08.030.

Grygorczuk, J., Banaszkiewicz, M., Kargl, G., Kömle, N.I., Ball, A.J., Seweryn, K., 2009a. Use of Hammering to determine cometary nucleus mechanical properties. In: Penetrometry in the Solar System II. Austrian Academy of Sciences Press, Vienna, pp. 93–108.

Grygorczuk, J., Seweryn, K., Wawrzaszek, R., Banaszkiewicz, M., 2009b. Technological features in the new mole penetrator KRET. In: Proceedings of the 13th European Space Mechanisms and Tribology Symposium, ESMATS 2009, Vienna, Austria, 25 September 2009 (ESA SP–670).

Hagermann, A., 2005. Planetary heat flow measurements. Philosophical Transactions of the Royal Society A 363, 277–2791. doi:10.1098/rsta.2005.1664.

Hagermann, A., Spohn, T., 1999. A method to invert MUPUS temperature recordings for the subsurface temperature field of P/Wirtanen. Advances in Space Research 23, 1333–1336. doi:10.1016/S0273-1177(99)00046-0.

Hagermann, A., Tanaka, S., Saito, Y., 2009. Thermal measurements on penetrators geometry sensitivity and optimization issues. In: Kargl, G., Kömle, N.I., Ball, A.J., Lorenz, R.D. (Eds.), Penetrometry in the Solar System II. Austrian Academy of Sciences Press, Vienna, pp. 109–122.

Hathi, B., Daniell, P.M., Banaszkiewicz, M., Hagermann, A., Leese, M.R., Zarnecki, J.C., 2007. Thermal conductivity instrument for measuring planetary atmospheric properties and data analysis technique. Journal of Thermal Analysis and Calorimetry 87, 585–590. doi:10.1007/s10973-006-7607-1.

Hathi, B., Ball, A.J., Banaszkiewicz, M., Daniell, P.M., Garry, J.R.C., Hagermann, A., Leese, M.R., Lorenz, R.D., Rosenberg, P.D., Towner, M.C., Zarnecki, J.C., 2008. Composition of Titan's lower atmosphere from in situ thermal conductivity measurements. Icarus 197, 579–584. doi:10.1016/j.icarus.2008.05.006.

Healy, J.J., de Groot, J.J., Kestin, J., 1976. The theory of the transient hot-wire method for measuring thermal conductivity. Physica B+C 82 (2), 392–408. doi:10.1016/0378-4363(76)90203-5.

Heiken, G., Vaniman, D., French, B., 1991. Lunar Sourcebook—A User's Guide to the Moon. Cambridge University Press, Cambridge (Available as CD from Lunar and Planetary Institute (LPI), Tucson, Arizona).

Horai, K., Fujimura, A., Tanaka, S., Mizutani, H., 1991. Measurement of the lunar regolith thermal conductivity in the Lunar-A mission. In: Abstracts of the Lunar and Planetery Science Conference, vol. 22, p. 589, Houston, Texas, September 1991 (Abstract available via NASA ADS).

Hütter, E.S., Kömle, N.I., Kargl, G., Kaufmann, E., 2008. Determination of the effective thermal conductivity of granular materials under varying pressure conditions. Journal of Geophysical Research 113, E12004. doi:10.1029/2008JE003085.

Hütter, E.S., 2007. Determination of the effective thermal conductivity of granular materials under atmospheric and vacuum conditions. Internal Report IWF#180 (Diploma Thesis, Karl-Franzens-University Graz, Austria), Space Research Institute, Austrian Academy of Sciences.

Hütter, E.S., 2011. Development and testing of thermal sensors for planetary applications. Ph.D. Thesis, Karl-Franzens-University Graz, Austria.

Incropera, F.P., DeWitt, D.P., Bergman, T.L., Lavine, A.S., 2007. Fundamentals of Heat and Mass Transfer, sixth ed. John Wiley Sons, New York.

Jaeger, J.C., 1941. Heat conduction in composite circular cylinders. Philosophical Magazine 32 (7, No. 213), 324–335. doi:10.1080/14786444108521306.

Jaeger, J.C., 1956. Conduction of heat in an infinite region bounded internally by a circular cylinder of a perfect conductor. Australian Journal of Physics 9, 167–179 CSIRO Australia (available via NASA ADS).

Jones, B.W., 1988. Thermal conductivity probe: development of method and application to a coarse granular medium. Journal of Physics E: Scientific Instruments 21, 832–839. doi:10.1088/0022-3735/21/9/002.

Kömle, N.I., Hütter, E.S., Kargl, G., Ju, H.H., Gao, Y., Grygorczuk, J., 2008. Development of thermal sensors and drilling systems for application on lunar lander missions. Earth, Moon and Planet 103, 119–141. doi:10.1007/s11038-008-9240-4.

Kömle, N.I., Bing, H., Feng, W.J., Wawrzaszek, R., Hütter, E.S., He, P., Marczewski, W., Dabrowski, B., Schröer, K., Spohn, T., 2007. Thermal conductivity measurements of road construction materials in frozen and unfrozen state. Acta Geotechnica 2, 127–138. doi:10.1007/s11440-007-0032-1.

Kömle, N.I., Huetter, E.S., Feng, W.J., 2010. Thermal conductivity measurements of coarse-grained gravel materials using a hollow cylindrical sensor. Acta Geotechnica 5, 211–223. doi:10.1007/s11440-010-0126-z.

Langseth, M.G. Jr., Clark, S.P. Jr., Chute, J.L. Jr., Kheim, S.J., Wechsler, A.E., 1972a. Chapter 11:11/1-11/23. Apollo 15 Preliminary Science Report: Heat Flow Experiment.

Langseth, M.G. Jr., Clark, S.P. Jr., Chute, J.L. Jr., Kheim, S.J., Wechsler, A.E., 1972b. Chapter 9:9/1-9/24. Apollo 17 Preliminary Science Report: Heat Flow Experiment.

Langseth, M.G. Jr., Clark, S.P. Jr., Chute, J.L. Jr., Kheim, S.J., Wechsler, A.E., 1972c. The Apollo 15 lunar heat flow measurement. Kluwer, NASA SP289, Washington DC, pp. 390–410.

Langseth, M.G., Keihm, S.J., Peters, K., 1976. Revised lunar heat-flow values. In: Lunar and Planetary Science Conference Proceedings, vol. 7, pp. 3143–3171.

Marczewski, W., Schröer, K, Seiferlin, K., Usowicz, B., Banaszkiewicz, M., Hlond, M., Grygorczuk, J., Gadomski, S., Krasowski, J., Gregorczyk, W., Kargl, G., Hagermann, A., Ball, A.J., Kührt, E., Knollenberg, J., Spohn, T., 2004. Prelaunch performance evaluation of the cometary experiment MUPUS-TP. Journal of Geophysical Research 109 (E7), 1–17. doi:10.1029/2003JE002192.

Mizutani, H., 1995. Lunar interior exploration by Japanese lunar penetrator mission Lunar-A. Journal of Physics of the Earth 43, 657–670.

Mizutani, H., Kohno, M., Nakajima, S., Fujimura, A., Kawaguchi, J., Saito, H., Hinada, M., 1995. Japanese lunar mission, Lunar-A. Acta Astronautica 35, 323–327. doi:10.1016/0094-5765(94)00197-T.

Özisik, M.N., 1989. Boundary Value Problems of Heat Conduction. Dover Phoenix Editions.

Paton, M.D., Kargl, G., Ball, A.J., Green, S.F., Hagermann, A., Kömle, N.I., Thiel, M., Zarnecki, J.C., 2010. Computer modelling of a penetrator thermal sensor. Advances in Space Research 46, 337–345. doi:10.1016/j.asr.2010.03.007.

Phylippov, L.P., Kravchun, S.N., Rleubaev, A.S., 1992. Apparatus for measuring thermophysical properties of liquids by AC hot wire techniques. In: Maglic, K.D. (Ed.), Compendium of Thermophysical Property Measurement Methods. Plenum Press, New York and London, pp. 375–405.

Richter, L., Coste, P., Gromov, V.V., Kochan, H., Nadalini, R., Ng, T.C., Pinna, S., Richter, H.-E., Yung, K.L., 2002. Development and testing of subsurface sampling devices for the Beagle-2 lander. Planetary Space Science 50, 903–913. doi:10.1016/S0032-0633(02)00066-1.

Grygorczuk, J., Seweryn, K., Rickman, H., Morawski, M., Aleksashkin, S.N., Banaszkiewicz, M., Dobrowolski, M., Drogosz, M., Gurgurewicz, J., Kozlov, O.E., Kozlova, T.O., Krolikowska-Soltan, M., Sutugin, S.E., Wawrzaszek, R., Wisniewski, L., Zakharov, A.V., 2010. CHOMIK sampling device for Russian Phobos Sample Return Mission, In: Proceedings of 1st Moscow Solar System Symposium, Moscow.

Seiferlin, K., 2006. The guarded torus: numerical model of a novel transient method for thermal conductivity measurements. Measurement Science and Technology 17, 3085–3093. doi:10.1088/0957-0233/17/11/029.

Seiferlin, K., Kömle, N.I., Kargl, G., Spohn, T., 1996. Line heat source measurements of porous H2O ice, CO2 ice, and mineral powders under space conditions. Planetary and Space Science 44, 691–704. doi:10.1016/0032-0633(96)00068-2.

Spohn, T., Ball, A.J., Seiferlin, K., Conzelmann, V., Hagermann, A., Kömle, N.I., Kargl, G., 2001. A heat flow and physical properties package for the surface of Mercury. Planetary and Space Science 49, 1571–1577. doi:10.1016/S0032-0633(01)00094-0.

Spohn, T., Seiferlin, K., Hagermann, A., Knollenberg, J., Ball, A.J., Banaszkiewicz, M., Benkhoff, J., Gadomski, S., Gregorczyk, W., Grygorczuk, J., Hlond, M., Kargl, G., Kührt, E., Kömle, N., Krasowski, J., Marczewski, W., Zarnecki, J.C., 2007. MUPUS—a thermal and mechanical properties probe for the Rosetta lander Philae. Space Science Reviews 128, 339–362. doi:10.1007/s11214-006-9081-2.

Schröer, K., 2006. Eine kompakte Sonde für Temperatur- und Wärmeleitfähigkeitsmessungen in dem Geowissenschaften. Ph.D. Thesis, Münster University, 2006, 203 pp.

Sullivan, A., 1994. Catalog of Apollo Experiment Operations. NASA RP-1317. NASA, Johnson Space Flight Center, Houston, Texas, pp. 61–65. URL: 〈www.lpi.usra.edu/lunar/documents/NASA%20RP-1317.pdf〉.

Tanaka, S., Yoshida, S., Hayakawa, M., Horai, K., Fujimura, A., Mizutani, H., 1999. Development of the heat flow measurement system by the LUNAR-A penetrators. Advances in Space Research 23, 1825–1828. doi:10.1016/S0273-1177(99)00535-9.

Teisseyre, R., Leliwa-Kopystynski, J., 1992. Evolution of the Earth and other Planetary bodies. PWN—Polish Scientific Publishers, Warszawa and Elsevier, Amsterdam, Oxford, New York, Tokyo.

Thiel, M., Stöcker, J., Rohe, C., Hillenmaier, O., Kömle, N.I., Kargl, G., 1999. The Rosetta lander anchoring harpoon: subsystem and scientific instrument. In: Penetrometry in the Solar System. Austrian Academy of Sciences Press, Vienna, pp. 137–149.

Vos, B.H., 1955. Measurements of thermal conductivity by a non-steady-state method. Applied Scientific Research 5, 425–438. doi:10.1007/BF03184603.

Wechsler, A.E., 1992. The probe method for measurement of thermal conductivity. In: Maglic, K.D. (Ed.), Compendium of Thermophysical Property Measurement Methods. Plenum Press, New York and London, pp. 161–185.

Woodfield, P.L., Fukai, J.F., Hujii, M., Takata, Y., Shinzato, K., 2008. A two-dimensional analytical solution for the transient short-hot-wire method. International Journal of Thermophysics 29, 1278–1298. doi:10.1007/s10765-008-0469-y.

Zarnecki, J.C., Leese, M.R., Hathi, B., Ball, A.J., Hagermann, A., Towner, M.C., Lorenz, R.D., McDonnell, J.A.M., Green, S.F., Patel, M.R., Ringrose, T.J., Rosenberg, P.D., Atkinson, K.R., Paton, M.D., Banaszkiewicz, M., Clark, B.C., Ferri, F., Marcello Fulchignoni, M., Ghafoor, N.A.L., Kargl, G., Svedhem, H., John Delderfield, J., Grande, M., Parker, D.J., Peter, G., Challenor, P.G., Geake, J.E., 2005. A soft solid surface on Titan as revealed by the Huygens surface science package. Nature 438, 792–795. doi:10.1038/nature04211.

Zent, A.P., Hecht, M.H., Cobos, D.R., Campbell, G.S., Campbell, C.S., Cardell, G., Foote, M.C., Wood, S.E., Mehta, M., 2009. Thermal and electrical conductivity probe (TECP) for Phoenix. Journal of Geophysical Research 114, E00A27. doi:10.1029/2007JE003052.

Zent, A.P., Hecht, M.H., Cobos, D.R., Wood, S.E., Hudson, T.L., Milkovich, S.M., DeFlores, L.P., Mellon, M.T., 2010. Initial results from the thermal and electrical conductivity probe TECP on Phoenix. Journal of Geophysical Research 115, E00E14. doi:10.1029/2009JE003420.